

# Genomic Mechanisms of Physiological and Morphological Adaptations of Limestone Langurs to Karst Habitats

Zhijin Liu,<sup>\*†,1,2</sup> Liye Zhang,<sup>†,1,3</sup> Zhongze Yan,<sup>†,1,2</sup> Zhijie Ren,<sup>†,4</sup> Fengming Han,<sup>†,5</sup> Xinxin Tan,<sup>1,3</sup> Zhiyuan Xiang,<sup>1,3</sup> Fang Dong,<sup>1,2</sup> Zuomin Yang,<sup>1,6</sup> Guangjian Liu,<sup>1</sup> Ziming Wang,<sup>1,3</sup> Jiali Zhang,<sup>1</sup> Tengcheng Que,<sup>7</sup> Chaohui Tang,<sup>8</sup> Yifeng Li,<sup>8</sup> Song Wang,<sup>9</sup> Junyi Wu,<sup>9</sup> Legong Li,<sup>4</sup> Chengming Huang,<sup>1</sup> Christian Roos,<sup>\*,10</sup> and Ming Li<sup>\*,1,11</sup>

<sup>1</sup>CAS Key Laboratory of Animal Ecology and Conservation Biology, Institute of Zoology, Beijing 100101, China

<sup>2</sup>Institute of Physical Science and Information Technology, Anhui University, Hefei 230601, China

<sup>3</sup>University of Chinese Academy of Sciences, Beijing 100049, China

<sup>4</sup>College of Life Sciences, Capital Normal University, Beijing 100048, China

<sup>5</sup>Biomarker Technologies Corporation, Beijing 101300, China

<sup>6</sup>School of Life Sciences, Qufu Normal University, Qufu 273165, Shandong, China

<sup>7</sup>Guangxi Zhuang Autonomous Region Terrestrial Wildlife Medical-Aid Monitoring Epidemic Diseases Research Center, Nanning 530001, Guangxi Province, China

<sup>8</sup>Wuzhou Langur Breeding and Research Center, Wuzhou 543002, Guangxi Province, China

<sup>9</sup>Nanning Zoo, Nanning 530000, Guangxi Province, China

<sup>10</sup>Gene Bank of Primates and Primate Genetics Laboratory, German Primate Center, Leibniz Institute for Primate Research, Göttingen 37077, Germany

<sup>11</sup>Center for Excellence in Animal Evolution and Genetics, Chinese Academy of Sciences, Kunming 650223, China

<sup>†</sup>These authors contributed equally to this work.

**\*Corresponding authors:** E-mails: lim@ioz.ac.cn; liuzj@ioz.ac.cn; croos@dpz.eu.

**Associate editor:** Connie Mulligan All data generated for this study have been submitted to the NCBI Sequence Read Archive (SRA) and NCBI genome (WGS) under BioProject PRJNA488530. ORCID: Z.L.: 0000-0003-2923-1120; C.R.: 0000-0003-0190-4266; M.L.: 0000-0001-5689-6270.

## Abstract

Knowledge of the physiological and morphological evolution and adaptation of nonhuman primates is critical to understand hominin origins, physiological ecology, morphological evolution, and applications in biomedicine. Particularly, limestone langurs represent a direct example of adaptations to the challenges of exploiting a high calcium and harsh environment. Here, we report a *de novo* genome assembly (Tfra\_2.0) of a male François's langur (*Trachypithecus francoisi*) with contig N50 of 16.3 Mb and resequencing data of 23 individuals representing five limestone and four forest langur species. Comparative genomics reveals evidence for functional evolution in genes and gene families related to calcium signaling in the limestone langur genome, probably as an adaptation to naturally occurring high calcium levels present in water and plant resources in karst habitats. The genomic and functional analyses suggest that a single point mutation (Lys1905Arg) in the  $\alpha 1c$  subunit of the L-type voltage-gated calcium channel  $Ca_v1.2$  (CACNA1C) attenuates the inward calcium current into the cells *in vitro*. Population genomic analyses and RNA-sequencing indicate that *EDNRB* is less expressed in white tail hair follicles of the white-headed langur (*T. leucocephalus*) compared with the black-colored François's langur and hence might be responsible for species-specific differences in body coloration. Our findings contribute to a new understanding of gene–environment interactions and physiomorphological adaptive mechanisms in ecologically specialized primate taxa.

**Key words:** *Trachypithecus*, nonhuman primates, langur genome, adaptive evolution, calcium signaling pathway, pelage coloration.

## Introduction

With more than 500 species, primates represent a diverse group of mammals (Mittermeier et al. 2013; Rowe and Myers 2016). Although humans have colonized all of earth's

extreme environments, nonhuman primates are mainly found in tropical, subtropical, and temperate regions. However, nonhuman primates also are highly adaptable and inhabit a broad range of environments including forests,

savannahs, mangroves, and semideserts (Groves 2001; Mittermeier et al. 2013; Rowe and Myers 2016). Adaptations of humans and nonhuman primates to severe ecological conditions have been increasingly investigated in recent years (Scheinfeldt and Tishkoff 2013). For instance, genomic studies in humans revealed hypoxic tolerance of Tibetan and other people living at high altitudes (Beall 2006), physiological adaptations to breath-hold diving of the Bajau people (“sea nomads”) (Ilardo et al. 2018), genomic signatures of adaptation to protein and fatty acid rich diets of the Inuit (Fumagalli et al. 2015), and local human populations exhibiting lighter or darker skin pigmentation as a response to different UV irradiation levels (Deng and Xu 2017).

Genomic evidence of adaptive evolution has also been reported in nonhuman primates. Gibbons, for example, appear to have adapted to their highly specialized form of bi-manual arm swinging arboreal locomotion (e.g., brachiation) by mutations in genes important for forelimb development and connective tissues (Carbone et al. 2014), tarsiers exhibit positive selection in genes associated with large eyes and nocturnality (Schmitz et al. 2016), and snub-nosed monkeys (*Rhinopithecus* spp.) living at high altitudes have adapted to this extreme environment by mutations in genes related to lung function and resistance to UV irradiation (Yu et al. 2016; Zhou et al. 2016). In Bornean orangutans (*Pongo pygmaeus*), positively selected genes (PSGs) are involved in fatty acid metabolism which has been hypothesized to be responsive to environmental fluctuations and unpredictable food supplies (Mattle-Greminger et al. 2018). The genome of the sooty mangabey (*Cercocebus atys*) revealed a frameshift mutation in the *TLR4* gene and a mutation in the *ICAM-2* gene that causes structural changes of the ICAM2 protein which may contribute to natural AIDS resistance (Palesch et al. 2018). Overall, knowledge of the patterns and processes underlying the evolution and adaptation of humans and nonhuman primates is critical for understanding hominin origins, physiological ecology, morphological evolution, and applications in biomedicine.

Limestone langurs are unique among primates in their ability to exploit karst formations in Southeast Asia. Karsts are distinctive landforms and hydrological systems formed by the dissolution of highly soluble and porous bedrock such as limestone (Ford and Williams 2007). Karst formations are typically steep, tall cliffs with only a thin, alkaline soil that is poor in nutrients except metal ion (calcium, magnesium, and sulfur; Clements et al. 2006). The seven allopatric species of limestone langurs (*T. francoisi*, *T. leucocephalus*, *T. poliocephalus*, *T. delacouri*, *T. hatinhensis*, *T. laotum*, and *T. ebenus*) belong to the Asian colobine genus *Trachypithecus* (Groves 2001; Mittermeier et al. 2013; Rowe and Myers 2016). The genus is widely distributed in Southeast Asia and contains 13 additional langur species, each of which inhabit forested nonkarst environments (Mittermeier et al. 2013; Rowe and Myers 2016). Based on biogeographical and phylogenetic evidence, the ancestors of *Trachypithecus* lived in forested environments, and according to similarities in morphology, ecology, behavior, distribution, and genetics, members of this genus can be grouped into four species groups of which three

occur mainly in forest habitats (*T. pileatus*, *T. obscurus*, and *T. cristatus* groups), while the limestone or *T. francoisi* group is restricted to karst habitats (Groves 2001; Osterholz et al. 2008; Workman 2010; Mittermeier et al. 2013). Limestone langurs typically sleep in caves or under rock shelters, and can easily walk, climb, and leap on sharp rocks, including steep vertical cliffs (Osterholz et al. 2008; Workman 2010; Mittermeier et al. 2013; Rowe and Myers 2016). They drink water from bole-like karst holes which contain high concentrations of minerals, particularly calcium (Huang and Li 2005; Hu 2007; Liu et al. 2016) and have been observed to lick limestone rock (Li et al. 2003; Zhou et al. 2006) (supplementary video 1, Supplementary Material online), exposing them to a generally high natural calcium intake. In addition, karst plant communities exhibit significantly higher levels of calcium compared with plants in other environments (Ji et al. 2009; Luo et al. 2012; Hao et al. 2015). For example, in the leaves of *Lonicera confusa*, one of the main food plants consumed by *T. francoisi* (Huang et al. 2008; Zhou et al. 2009), calcium is transported to the glands, epidermal hairs and stomata of the leaves (Workman and Dung 2009; Wu et al. 2011; Jin et al. 2018). Phenotypically, all seven species of limestone langurs exhibit generally black fur coloration, but species differ in the extent of white or golden parts on the head, rump, or tail (Rowe and Myers 2016); a potential camouflage in white, yellowish, and black rock formations (Huang 2011; Huang et al. 2016).

Although various primate genomes have been sequenced, genome sequence information for langurs of the genus *Trachypithecus* is lacking. Therefore, we sequenced and de novo assembled the genome of a male François’s langur (*T. francoisi*) using a combination of high-fidelity short-read sequencing (Illumina HiSeq Xten), long-read single-molecule sequencing (PacBio RSII), and Hi-C-based chromatin interaction maps (Phase Genomics, Inc.). The postfiltered data provided  $\sim 279\times$  average coverage across 2.87 Gb of assembled sequence. For comparative reasons, we also generated whole-genome shotgun (WGS) short-read data (Illumina) for 23 additional langur individuals representing five limestone (*T. francoisi*, *T. leucocephalus*, *T. hatinhensis*, *T. laotum*, and *T. ebenus*) and four forest langur species (*T. phayrei* and *T. obscurus* of the *T. obscurus* group, *T. auratus* and *T. germaini* of the *T. cristatus* group) (supplementary fig. S1, Supplementary Material online). Specifically, we aimed to uncover specific adaptations and the underlying gene changes related to calcium tolerance, the ability to travel, climb, and leap on vertically steep rock surfaces, and variation in coat coloration in limestone langurs.

## Results

### De Novo Sequencing, Assembly, Annotation, and Resequencing

We sequenced the genome of a male François’s langur using a combined strategy and generated 598.37 Gb data from Illumina short reads of mate pair libraries ranging from 180 bp to 15 kb, 272.97 Gb data from PacBio long reads with a mean read length of 10,495 kb, and 151.6 Gb Hi-C data (supplementary tables S1–S5, Supplementary Material

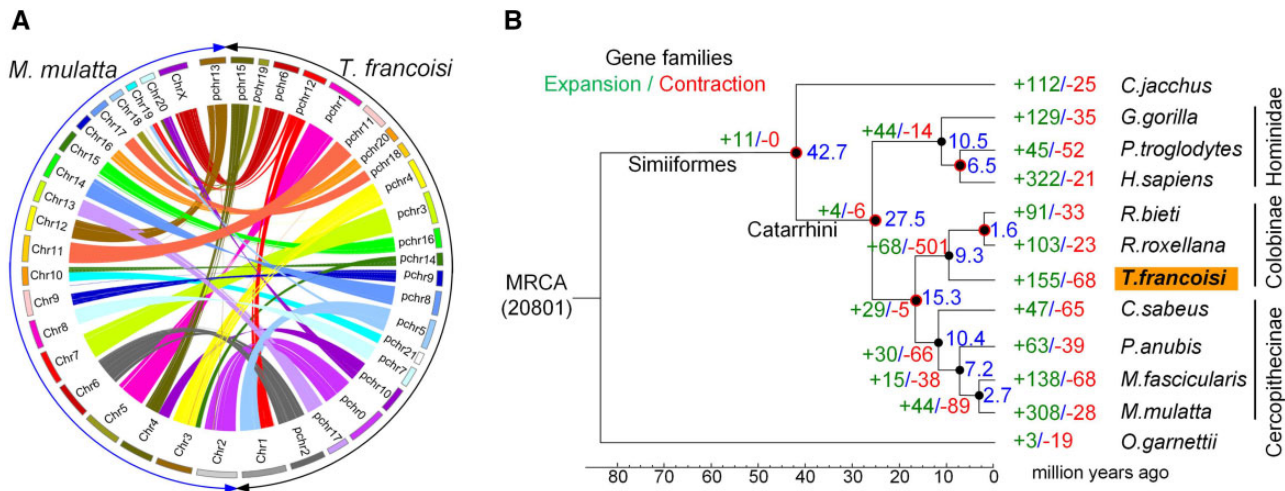


**Fig. 1.** Comparative genomics analyses of *Trachypithecus francoisi*. (A) Whole-genome synteny analysis for *T. francoisi* and *Macaca mulatta*. Most *T. francoisi* pseudochromosomes (pchr0–pchr21) show high collinearity with the *M. mulatta* genome (chr1–chrX). (B) Phylogenomic relationships among 12 primate species and gene family expansions and contractions in the *T. francoisi* genome. The numbers on branches correspond to the numbers of orthologous gene families that have expanded (green) and contracted (red). Orthologous gene families across 12 primates were defined using TreeFam (Li et al. 2006). The expanded and contracted gene families on the branch leading to *T. francoisi* are described in supplementary tables S23 and S26 (Supplementary Material online). Blue numbers correspond to the divergence time between species. The divergence times between species were estimated with mcmctree in PAML 4 (Yang 2007). Calibration points (red cycled points) used in Perelman et al. (2011) and Yu et al. (2016) were applied as normal priors. Black dots at nodes refer to bootstrap values >95%.

online). We obtained a 2.87 Gb assembled sequence of the langur genome, with an N50 of 16.3 Mb in the final assembly (Tfra\_2.0) (supplementary table S8, Supplementary Material online). The contigs were further assembled into chromosome-scale pseudomolecules (pseudochromosomes, pchrs) that were on the order of the length of full chromosomes (supplementary table S9, Supplementary Material online). The genomic synteny between pchrs of the *T. francoisi* genome and chromosomes of the rhesus monkey (*Macaca mulatta*) was evaluated (fig. 1A and supplementary table S11, Supplementary Material online). A total of 25,421 protein-coding genes were annotated in the langur genome (98.01% of which were functionally classified; supplementary tables S13 and S14, Supplementary Material online). Furthermore, 23 samples from five limestone (*T. francoisi*, *T. leucocephalus*, *T. hatinhensis*, *T. laotum*, and *T. ebenus*) and four forest langur species (*T. phayrei*, *T. obscurus*, *T. auratus*, and *T. germaini*) were collected and the genomes were resequenced at a high average depth of  $30.79 \pm 4.73\times$  with an overall average genome coverage of  $98.52\% \pm 0.32\%$  of the langur reference genome, and a total of 48,659,471 single nucleotide polymorphisms (SNPs) was identified and used for downstream analyses (supplementary tables S16 and S17, Supplementary Material online).

### Orthologous Gene Family and Phylogenetic Tree Construction

The protein-coding genes of *T. francoisi* and 11 other primate species (*Homo sapiens*, *Pan troglodytes*, *Gorilla gorilla*, *M. mulatta*, *M. fascicularis*, *Papio anubis*, *Chlorocebus sabaues*, *Rhinopithecus roxellana*, *R. bieti*, *Callithrix jacchus*, and *Otolemur garnettii*) were clustered into 20,801 orthologous

groups using TreeFam (Li et al. 2006). About 10,280 shared single-copy gene orthologs were detected in *T. francoisi* and the 11 other primates. Using the shared single-copy protein-coding genes, we reconstructed a timescale for primate evolution and estimated the divergence time between *T. francoisi* and *R. roxellana*, another Asian colobine genus, at  $9.30 \pm 3.30$  Ma. Based on this tree, we determined orthologous gene families that experienced expansion and contraction in the investigated primates (fig. 1B).

### Identification of PSGs and Enrichment Analysis

Using the branch-site likelihood ratio test (Yang 2007), we identified 130 PSGs in the *T. francoisi* genome compared with the above-mentioned 11 primate species (supplementary table S18, Supplementary Material online). The analysis of langur resequencing data revealed that 56 of these 130 PSGs are shared by limestone and forest langurs, another 56 are private to all 5 investigated limestone langur species, 5 are shared by *T. francoisi* and *T. leucocephalus*, and 13 were found only in *T. francoisi* (supplementary table S18 and fig. S10, Supplementary Material online). Consequently, the 56 PSGs found in all five limestone langur species and not present in any forest langur were regarded as potential targets of positive selection in all limestone langurs. These 56 PSGs private to all limestone langurs show an overrepresentation in the Kyoto Encyclopedia of Genes and Genomes (KEGG) pathways of “calcium signaling” and “oxytocin signaling,” and Gene Ontology (GO) terms related to circulatory system and skeletal system, such as “vasoconstriction,” “blood circulation,” and “limb morphogenesis,” implying potential physiological and morphological adaptations of limestone langurs to karst

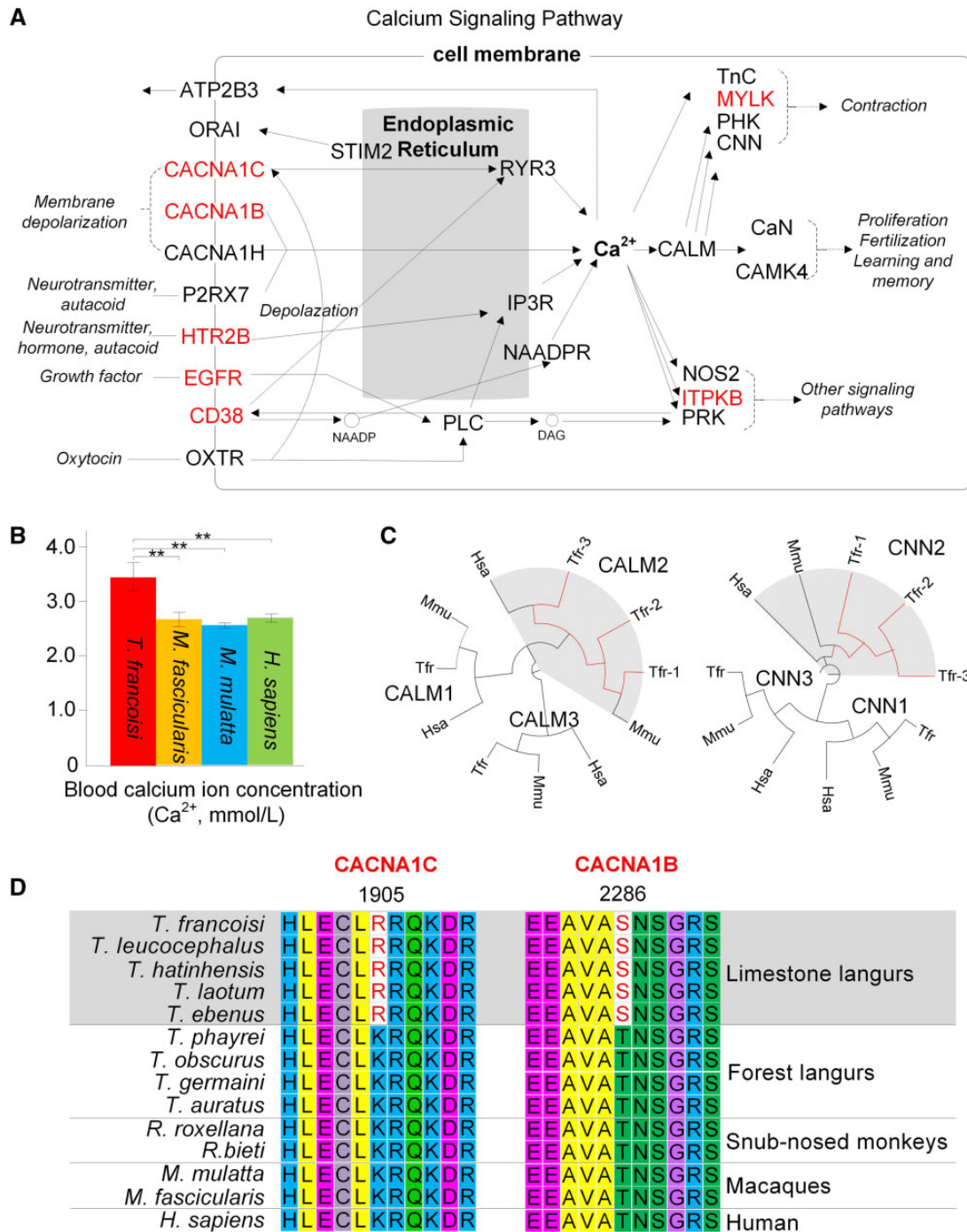


**Fig. 2.** Genomic adaptation to high blood calcium ion concentration in limestone langurs. (A) Enrichment for PSGs that function in calcium signaling pathway. PSGs in *Trachypithecus francoisi* are shown in red. (B) Comparison of blood calcium ion concentration among *T. francoisi*, *Macaca fascicularis*, *M. mulatta*, and *Homo sapiens* (\*\* $P < 0.01$ ). (C) Unrooted neighbor-joining trees constructed using expanded CALM2 and CNN2 gene families in *T. francoisi* (Tfr, red branches) and orthologs in rhesus monkey (Mmu) and human (Hsa). Genes with red branch in gray shaded areas indicate subtypes that experienced expansion. (D) The sequence alignments of CACNA1C and CACNA1B show sites 1905 and 2286 identified as positively selected amino acids in limestone langurs.

habitats (all  $P < 0.05$ , Fisher's exact test; [supplementary tables S19 and S20](#), [Supplementary Material](#) online).

### Positively Selected Genes Related to $Ca^{2+}$ Signaling Pathway

The KEGG pathway of the “calcium signaling pathway” was enriched with seven genes (CACNA1C, CACNA1B, CD38,

EGFR, HTR2B, ITPKB, and MYLK; false discovery rate (FDR) adjusted  $P < 0.05$ , Fisher's exact test; [fig. 2A](#) and [supplementary table S19](#), [Supplementary Material](#) online). For instance, CACNA1C codes for the L-type voltage-gated calcium channel  $Ca_v1.2$ , which is the predominant calcium channel with long-lasting inward current and large conductance, while CACNA1B codes for a presynaptic neuronal voltage-gated

**Table 1.** Private Amino Acid Substitutions in the PSGs Involved in the Calcium Signaling and Oxytocin Signaling Pathways of Limestone Langurs and the Allele Frequencies in Human ExAC Database.

Gene Symbol	Substitutions in Limestone Langurs	Orthologous Variants in Humans	Allele Frequency in Humans
CACNA1C	1905 K/R	chr12: 2795365 A/G	0.00000828
CACNA1B	2286 T/S	chr9: 141016288 C/G	None
CD38	245 G/V	chr4: 15841723 G/T	None
EGFR	560 P/S	chr7: 55231472 C/T	0.00000828
ITPKB	162 Q/H	chr1: 226736974 T/A	None
MYLK	470 H/Y	chr3: 123451851 G/A	None
HTR2B	3546 T/M	chr15: 34110816 C/T	0.00002501

ExAC, The Exome Aggregation Consortium.

calcium channel  $Ca_v2.2$  (Heyes et al. 2015; Plumbly et al. 2019). Both channels control depolarization-induced inward calcium currents into the mammalian cells and play an important role in dendritic development, neuronal survival, synaptic plasticity, memory formation, learning, and behavior (Winder and Walsh 1993; Barad 2003; Lipp and Reither 2011). The other five PSGs also play important roles in the regulation of calcium homeostasis in the cytoplasm and organelles through modulating calcium ion transportation (Clapham 2007; Wang et al. 2017; Bäder et al. 2018). In each of these seven genes, we observed one positively selected amino acid substitution in *T. francoisi*, and the allele frequencies of these substitutions are extremely low (0–0.000025) in human populations according to the Exome Aggregation Consortium (ExAC) (Lek et al. 2016), indicating these seven amino acid positions are highly conserved in humans (table 1). In most primates, blood  $Ca^{2+}$  concentrations range from 2.15 to 2.83 mmol/l (Teare 2002). Limestone langurs, however, have to cope with their naturally high calcium ion ( $Ca^{2+}$ ) intake. Consistently, the blood  $Ca^{2+}$  concentration of *T. francoisi* is significantly higher ( $3.31 \pm 0.27$  mmol/l) than in *H. sapiens* ( $2.53 \pm 0.11$  mmol/l), *M. mulatta* ( $2.43 \pm 0.08$  mmol/l), and *M. fascicularis* ( $2.56 \pm 0.12$  mmol/l) (all  $P < 0.01$ , Student's *t*-test; fig. 2B and supplementary table S21, Supplementary Material online). We further checked for the presence of these 7 amino acid substitutions in other limestone langurs, 4 forest langurs (*T. phayrei*, *T. obscurus*, *T. auratus*, and *T. germaini*), 2 snub-nosed monkeys (*R. bieti* and *R. roxellana*), 2 macaques (*M. mulatta* and *M. fascicularis*), human, and 11 other primates (*P. troglodytes*, *G. gorilla*, *Pongo abelii*, *Nomascus leucogenys*, *P. anubis*, *P. hamadryas*, *C. sabaeus*, *C. jacchus*, *Saimiri boliviensis*, *M. murinus*, and *O. garnettii*), and found them to be present in all limestone langurs, but not in any other primate species (fig. 2D for CACNA1C and CACNA1B and supplementary table S22, Supplementary Material online, for all seven genes), implying a potential adaptation of limestone langurs to a high calcium ion extracellular environment.

As the  $Ca_v1.2$  channel is the predominant calcium channel, we tested the effects of the substitution Lys1905Arg/K1905R of CACNA1C on the  $Ca_v1.2$  channel activity. We expressed CACNA1C and CACNA1C-K1905R in *Xenopus laevis* oocytes, and measured their channel activities by Two-Electrode Voltage-Clamp (TEVC) technology (fig. 3A). We found that the inward current produced by CACNA1C-K1905R is significantly smaller than that of CACNA1C (fig. 3B and C).

Furthermore, we delivered the shuttle plasmids containing the coding sequences (CDS) of CACNA1C and CACNA1C-K1905R into human embryonic kidney 293FT cells (HEK293FT, Sci-Tech, Shanghai, China) using lentivirus package methods and generated overexpressed cells (fig. 3D–F). Through calcium imaging, we found that CACNA1C-K1905R attenuates the inward calcium current into cells compared with the reference CACNA1C protein (fig. 3G), suggesting that the K1905R substitution of CACNA1C is critical to reduce channel activity, and is likely to contribute to increased resistance against high  $Ca^{2+}$  concentrations (fig. 3H).

### Positively Selected Genes Related to Oxytocin Signaling Pathway

The KEGG pathway of “oxytocin signaling” was enriched with four genes which are all also involved in the  $Ca^{2+}$  signaling pathway (CACNA1C, CD38, EGFR, and MYLK; FDR adjusted  $P < 0.05$ , Fisher's exact test; fig. 2A and supplementary fig. S11 and tables S19 and S22, Supplementary Material online). The binding of oxytocin to oxytocin receptor (OXTR) located on cytomembrane stimulates an increase of intracellular calcium by the inward calcium current into cells through L-type  $Ca^{2+}$  channels and calcium release from the endoplasmic reticulum (fig. 2A; Berrada et al. 2000; Lee et al. 2008). As mentioned earlier, CACNA1C, which codes for the L-type  $Ca^{2+}$  channel Cav1.2, and other three genes are also involved in the regulation of intracellular calcium levels through modulating the calcium ion transportation (Minton 2014; Wang et al. 2017). For example, MYLK encodes for the myosin light chain kinase, a calcium/calmodulin-dependent Ser (serine)/Thr (threonine) protein kinase, which mediates a store-operated calcium entry (Minton 2014). It is thus reasonable to hypothesize that positively selected amino acid sites in these PSGs regulate the intracellular calcium level in limestone langurs as an adaptive mechanism for high  $Ca^{2+}$  concentrations.

### Orthologous Gene Family Evolution

In total, we identified 155 gene families that were expanded in *T. francoisi* after the divergence from the lineage leading to the snub-nosed monkeys (*R. bieti* and *R. roxellana*), and 114 of them expanded before the divergence between limestone and forest langurs (supplementary table S23 and fig. S12, Supplementary Material online). We found substantial expansion of orthologous gene families in both limestone and forest langur genomes that are involved in the GO terms of “regulation of muscle adaptation” and “regulation of muscle

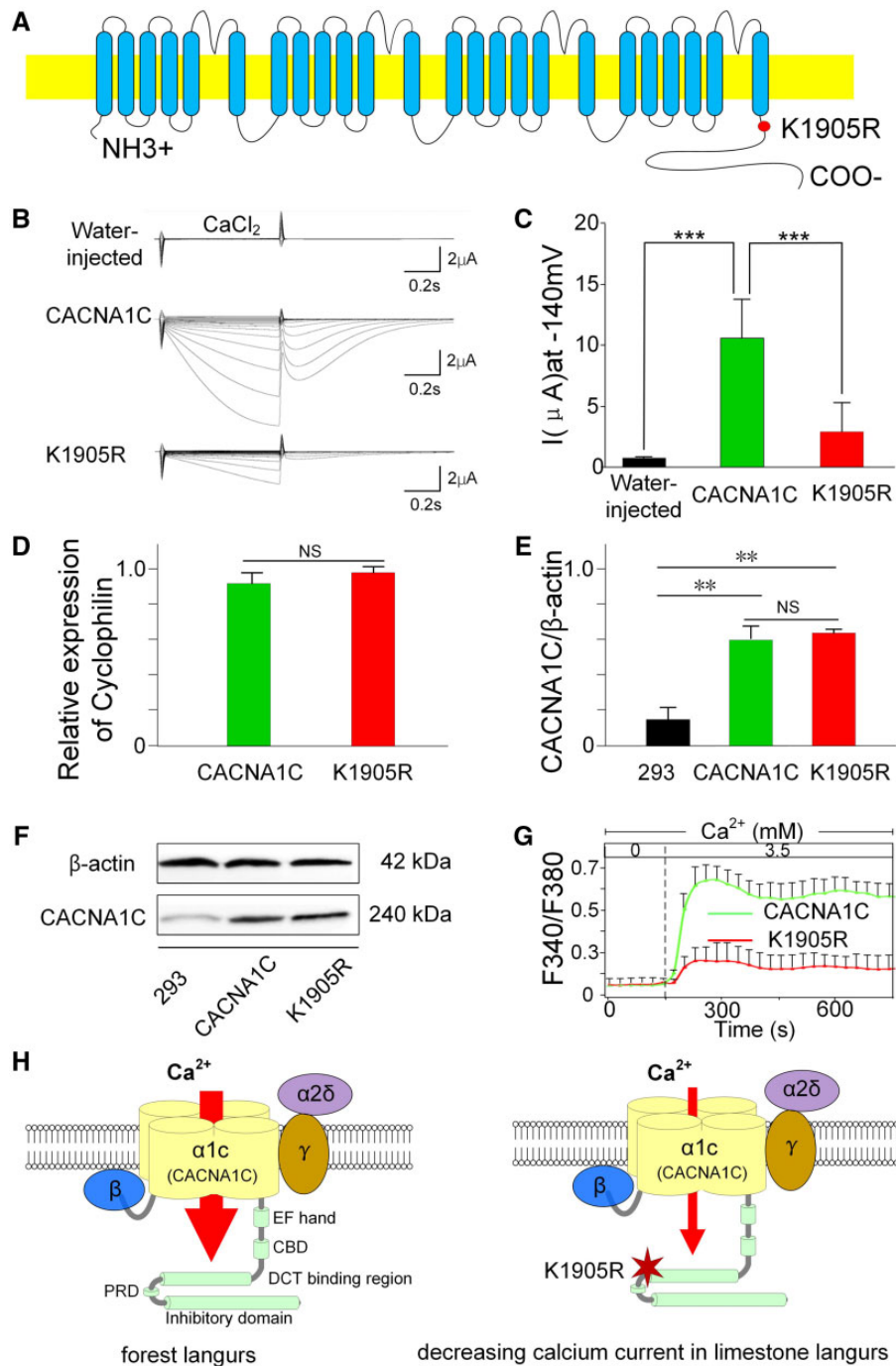


**Fig. 3.** Functional experiments of CACNA1C. (A) The protein structure of CACNA1C ( $\alpha 1c$  subunit of the Cav1.2 channel) and K1905R mutation in the distal C terminus of the CACNA1C of limestone langurs. (B) TEVC recording of inward current from *Xenopus* oocytes expressing CACNA1C, CACNA1C-K1905R, and water-injected control. (C) Current amplitudes at  $-140$  mV from multiple recordings as in (B) (\*\*\* $P < 0.001$ , NS, not significant, two-sided Student's  $t$ -test). (D) qPCR analysis of CACNA1C of cultured CACNA1C and CACNA1C-K1905R cells (NS, not significant, two-sided Student's  $t$ -test). (E) and (F) Western-blot analysis and quantification of CACNA1C expression levels in negative control HEK293FT, CACNA1C, and CACNA1C-K1905R cells (\*\* $P < 0.01$ , NS, not significant, two-sided Student's  $t$ -test). (G) Intracellular Ca<sup>2+</sup> concentration change from Ca<sup>2+</sup> free HBSS to 3.5 mM Ca<sup>2+</sup> HBSS in CACNA1C and CACNA1C-K1905R cells ( $n = 6$ , respectively). F340/F380 is the ratio of Fura-2 signals at 340 and 380 nm excitation wavelengths which was used to indicate the cytosolic Ca<sup>2+</sup> concentration (Tang et al. 2003; Wang et al. 2016). (H) Schematic presentation of the 3D Cav1.2 channel and the function of decreasing calcium current into cells caused by the K1905R mutation.  $\alpha 2\delta$ ,  $\beta$ , and  $\gamma$  indicate the auxiliary  $\alpha 2\delta$ ,  $\beta$ , and  $\gamma$  subunits of Cav1.2 channel. EF-hand, helix E-loop-helix F structural domain (1526–1554 aa); CBD, calmodulin binding domain (1588–1669 aa); DCT binding region, distal C terminus binding region (1733–1905 aa); PRD, proline-rich domain (1974–2000 aa); inhibitory domain (2024–2171 aa) (revised from Kim et al. 2004; Qian et al. 2017).

contraction" (all FDR  $P < 0.05$ , Fisher's exact test; [supplementary table S24, Supplementary Material](#) online). For example, *CALM2* and *CNN2* are expanded to three copies in both limestone and forest langur genomes, and several amino acid changes occurred leading to increased diversity of both gene families in langurs compared with other primates ([fig. 2C and supplementary figs. S13 and S14, Supplementary Material](#) online). Eight expanded gene families were only found in all five limestone langurs, implying that these gene families expanded in the common ancestor of the limestone langurs and after the divergence from forest langurs ([supplementary table S23, Supplementary Material](#) online). Among them, 17 genes that show an overrepresentation in categories involved in metal ion metabolism, such as GO terms of "iron ion binding" and "cation transport" (all FDR  $P < 0.05$ , Fisher's exact test; [supplementary table S25, Supplementary Material](#) online).

On the other side, we identified 68 orthologous gene families that were contracted in *T. francoisi* after the divergence from the lineage leading to the snub-nosed monkeys (*R. bieti* and *R. roxellana*). There are nine orthologous gene families that contracted after the divergence of forest and limestone langurs and before limestone langur species diverged from each other, implying that the contraction occurred in the common ancestor of limestone langurs ([supplementary table S26 and fig. S15, Supplementary Material](#) online). One of these nine contracted orthologous gene families is "Myotubularin-like phosphatase," which is involved in intracellular  $\text{Ca}^{2+}$  homeostasis ([Weiss et al. 2009; Romero-Suarez et al. 2010](#)).

### Phylogenetic Relationships and Demographic History of Limestone and Forest Langurs

To explore the phylogenetic relationships among langur species, we reconstructed a neighbor-joining tree using autosomal SNPs and estimated divergence times. We revealed a divergence time for the split of limestone langurs from forest langurs at 2.90 Ma (95% HPD 2.23–3.56) and the age of the most recent common ancestor of extant limestone langurs at 1.13 Ma (95% HPD 0.76–1.67; [fig. 4A and supplementary fig. S20, Supplementary Material](#) online). As expected, the principal component analysis (PCA; [Pearson 1901](#)) recapitulated the results of the phylogenetic tree ([fig. 4B](#)). The first eigenvector separated limestone and forest langurs (variance explained = 21.12%, Tracy–Widom test  $P = 4.7 \times 10^{-2}$ ), while the second eigenvector separated the *T. obscurus* group (*T. phayrei* and *T. obscurus*) and *T. cristatus* group (*T. auratus* and *T. germaini*) (variance explained = 12.32%, Tracy–Widom test  $P = 2.21 \times 10^{-1}$ ; [fig. 4B and supplementary table S28, Supplementary Material](#) online). To infer the demographic history of langurs, we applied a pairwise sequential Markovian coalescent (PSMC) ([Li and Durbin 2011](#)) analysis based on the distribution of heterozygous sites across the genome ([fig. 4C and D and supplementary fig. S23, Supplementary Material](#) online). The early demographic history of langurs is marked by population fluctuations following the glacial periods during the Pleistocene. Most forest and limestone langurs experienced a population reduction at the time of the Xixiabangma Glaciation (XG, 1,170–800 ka),

followed by an expansion during the Mid-Pleistocene interglaciation (800–200 ka). The second decline occurred ~200 ka coinciding with the Penultimate Glaciation (PG, 200–130 ka) and the Last Glaciation (LG, 70–10 ka) ([fig. 4C and D; Zheng et al. 2002](#)).

### Divergence between *T. francoisi* and *T. leucocephalus* and Genomic Mechanism of Pelage Color Variation

The divergence between *T. francoisi* and *T. leucocephalus* (white-headed langur) was estimated to have occurred 0.35 Ma (95% HPD, 0.11–0.72; [fig. 4A and supplementary fig. S20, Supplementary Material](#) online). To further investigate the divergence between *T. francoisi* and *T. leucocephalus* on a population genomic level and to trace genomic mechanism of variation in pelage coloration, we further launched population genomic analysis using eight *T. francoisi* and eight *T. leucocephalus* individuals from two sites each ([fig. 4E](#)). In the phylogenomic tree ([fig. 4F and supplementary fig. S20, Supplementary Material](#) online), individuals of *T. francoisi* and *T. leucocephalus* formed reciprocally monophyletic clades. Next, we performed a population structure analysis using *frappe* ([Tang et al. 2005](#)). When  $K = 2$ , individuals of *T. francoisi* and *T. leucocephalus* represented two distinct populations, while when  $K = 4$ , both species further segregated into two clades referring to geographic sites ([fig. 4F](#)). We further conducted PCAs. The first eigenvector separated *T. francoisi* and *T. leucocephalus* (variance explained = 6.69%, Tracy–Widom test  $P = 3.18 \times 10^{-3}$ ), while the second eigenvector separated the two disjunct *T. francoisi* subpopulations (variance explained = 4.04%, Tracy–Widom test  $P = 4.60 \times 10^{-2}$ ) ([fig. 4G and supplementary table S29, Supplementary Material](#) online).

To determine the genomic regions under selection between *T. leucocephalus* and *T. francoisi* ([fig. 5A](#)) on a population genomic level, we identified putative targets of selection by carrying out pairwise comparisons between both species using the fixation index ( $F_{ST}$ ) and genetic diversity ( $\theta_{\pi}$ ), calculated on 50 kb long sliding windows ([fig. 5B and C](#)). The top 5% of the windows with the largest  $F_{ST}$  and background/target  $\theta_{\pi}$  log-ratios in comparison were considered to be potentially under a selective sweep ([Qiu et al. 2015; Yang et al. 2016](#)). Furthermore, we estimated the cross-population extended haplotype homozygosity (XP-EHH; [Sabeti et al. 2007](#)) statistic for *T. leucocephalus*, using the control group (*T. francoisi*) as a reference and applying the top 5th percentile outliers as threshold to identify candidate genes ([fig. 5D](#)). Eighty-seven candidate genes under selective sweep were identified through the overlap of  $F_{ST}$ ,  $\theta_{\pi}$  ratio, and XP-EHH analyses, which are expected to represent targets of selection in *T. leucocephalus* ([fig. 5E and supplementary table S30, Supplementary Material](#) online). Functional classification and enrichment analyses of these 87 candidate genes under selective sweep were performed using KOBAS 3.0 ([Xie et al. 2011](#)). These 87 genes show an overrepresentation in the KEGG pathway of "Inflammatory mediator regulation of TRP channels," "Melanogenesis," and "Ribosome biogenesis in eukaryotes," and GO terms of "Defense response to Gram-negative bacterium," "Collagen catabolic process," and

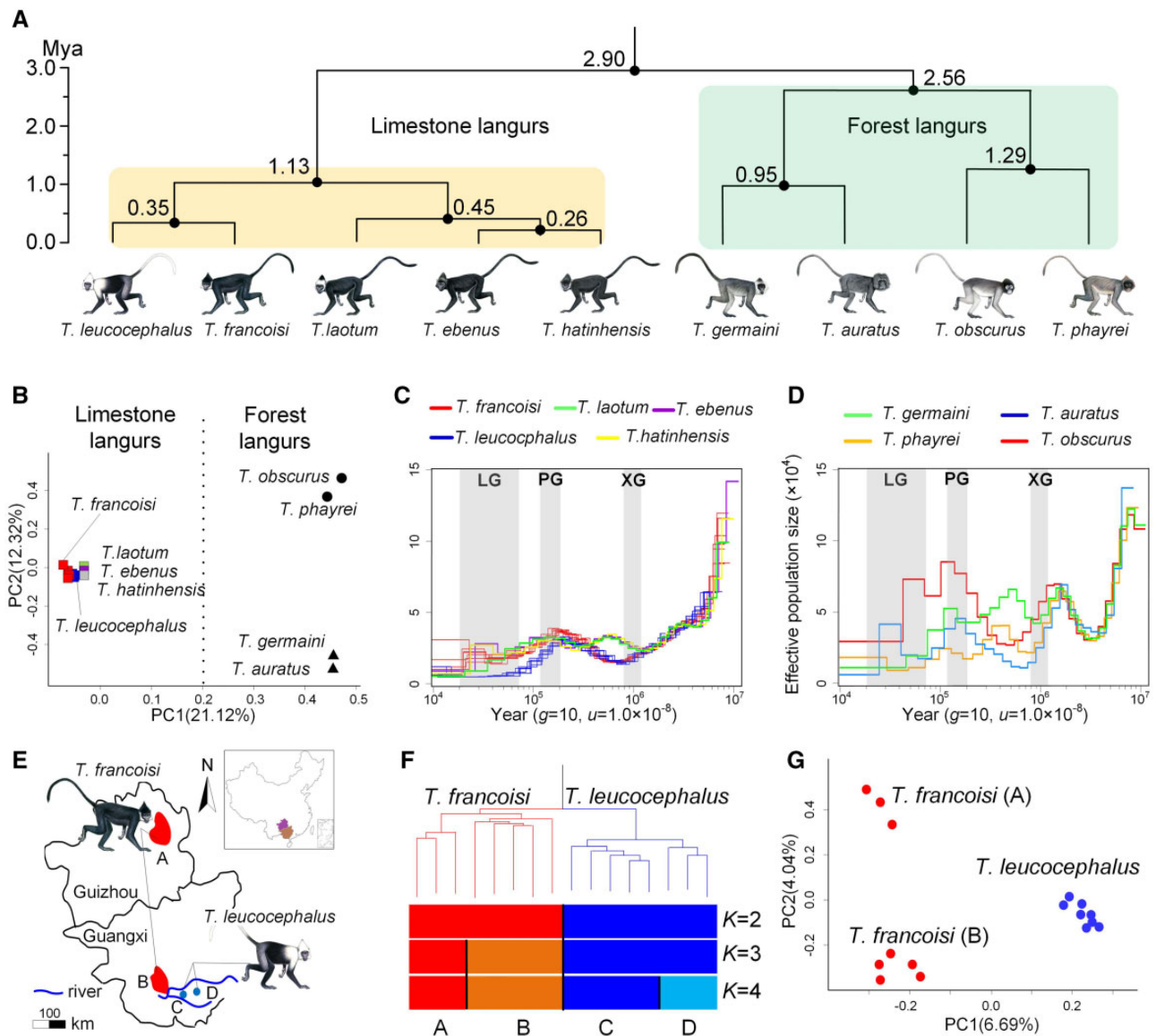


**FIG. 4.** Phylogenetic relationships and demographic histories of langurs. (A) Time-calibrated phylogeny based on autosomal SNP data of nine langur species. All nodes gained bootstrap values >95%. Numbers at nodes refer to divergence times. (B) PCA plots of the first two components among forest and limestone langurs. The fraction of the variance explained is 21.12% for PC1 (Tracy–Widom test  $P < 0.05$ ) and 12.32% for PC2 (Tracy–Widom test  $P = 0.22$ ; [supplementary table S28](#), [Supplementary Material](#) online). Red, blue, green, purple, and gray squares refer to *Trachypithecus francoisi*, *T. leucocephalus*, *T. laotum*, *T. ebenus*, and *T. hatinhensis* individuals, respectively. (C) Demographic histories of four forest and (D) five limestone langur species reconstructed using the PSMC model ( $g$  [generation time] = 10 years;  $\mu$  [neutral mutation rate per generation] =  $1.0 \times 10^{-8}$ ). The period of the Xixiabangma Glaciation (XG, 1,170–800 ka), Penultimate Glaciation (PG, 200–130 ka), and the Last Glaciation (LG, 70–10 ka) are shaded in gray. (E) Distribution and sampling sites of *T. francoisi* and *T. leucocephalus*. (F) A neighborhood-joining tree constructed using autosomal SNP data of *T. francoisi* and *T. leucocephalus* and population structure plots with  $K = 2$ –4. (G) PCA plots of the first two components among eight *T. francoisi* and eight *T. leucocephalus* individuals. The fraction of the variance explained is 6.69% for PC1 and 4.04% for PC2, with Tracy–Widom test  $P < 0.05$  ([supplementary table S29](#), [Supplementary Material](#) online). Illustrations copyright 2013 Stephen D. Nash/IUCN SSC Primate Specialist group. Used with permission.

“Adherens junction organization” ([supplementary table S31](#), [Supplementary Material](#) online). Interestingly, the term of “hair color” in the National Human Genome Research Institute (NHGRI) GWAS Catalog was enriched with one gene *EDNRB* ( $P < 0.05$ , Fisher’s exact test; [supplementary table S31](#), [Supplementary Material](#) online). *EDNRB* plays a vital role in the “melanogenesis” (04916) KEGG pathway ([fig. 5F](#)) and is reported to be responsible for white spotted coloration

on the head of various species, for example, Waardenburg syndrome type 4 (WS4) in humans ([Puffenberger et al. 1994](#)), aganglionosis in rats ([Garipey et al. 1996](#)), piebald-lethal in mice ([Hosoda et al. 1994](#)), lethal white foal syndrome in horses ([Metallinos et al. 1998](#)), and panda plumage color phenotype in Japanese quails ([Miwa et al. 2007](#)). Yoshihara et al. have reported a 50 kb deletion in the intergenic region ~50 kb upstream of *EDNRB* which causes white spots on the

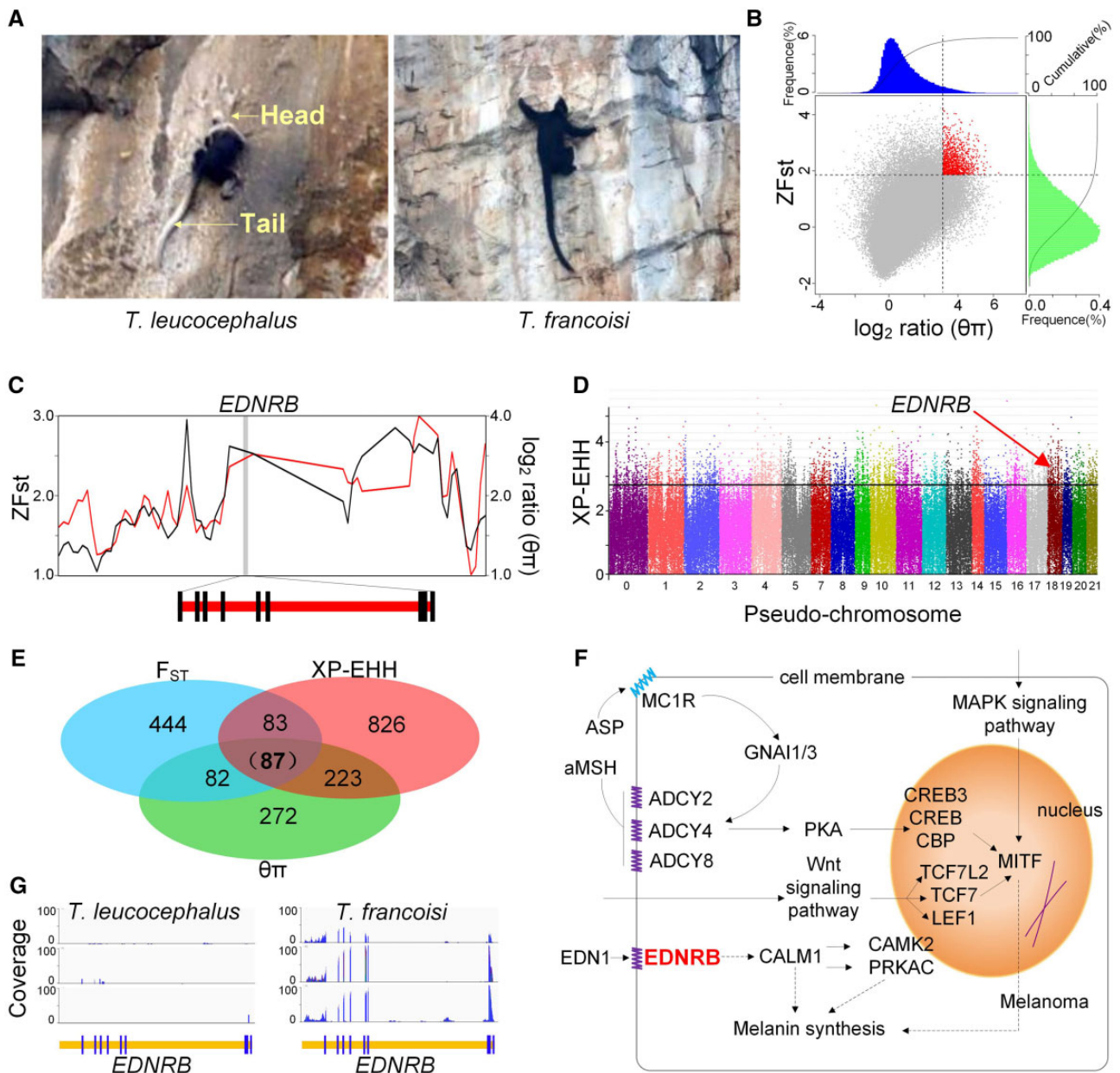


**Fig. 5.** Genomic mechanism underlying coat color variation in *Trachypithecus francoisi* and *T. leucocephalus*. (A) Photos of *T. leucocephalus* and *T. francoisi* individuals in karst habitat. (B) Distribution of  $Z(F_{ST})$  and  $\log_2$  ratio ( $\theta_{\pi, T. francoisi} / \theta_{\pi, T. leucocephalus}$ ) values (indicated by green and blue colors, respectively) calculated in 50 kb sliding windows with 25 kb increments between *T. francoisi* and *T. leucocephalus*. The data points in red (corresponding to the top 5% of the empirical  $\log_2$  ( $\theta_{\pi}$ ) ratio distribution with values  $>2.67$  and the top 5% of the empirical  $Z(F_{ST})$  distribution with values  $>1.83$ ) are genomic regions under selection in *T. leucocephalus*. (C)  $Z(F_{ST})$  and  $\log_2$  ( $\theta_{\pi}$ ) ratios around *EDNRB* in *T. leucocephalus*. The red and black lines represent the  $Z(F_{ST})$  and  $\log_2$  ( $\theta_{\pi}$ ) values, respectively. The red horizontal line and the black bars under the graphs of  $Z(F_{ST})$  and  $\log_2$  ( $\theta_{\pi}$ ) ratios indicate the gene structures in which black bars refer to exons. (D) Genomic landscape of the XP-EHH values in the genome of *T. leucocephalus* (top 5% outliers, XP-EHH value  $>2.67$ ). (E) Number of candidate genes under selective sweep identified in *T. leucocephalus* by the three methods listed in each of the Venn diagram components. Numbers in parentheses show the number of candidate genes in [supplementary table S30 \(Supplementary Material online\)](#). (F) The signaling pathway for hair color and melanogenesis synthesis regulation. The selected candidate genes are shown in red. (G) *EDNRB* transcript coverage from RNA-seq data of tail hair follicles of *T. leucocephalus* and *T. francoisi* (three individuals for each species).

head of rats (Yoshihara et al. 2017). Using RNA-seq data, we also found that *EDNRB* is less expressed in tail hair follicles of *T. leucocephalus* compared with *T. francoisi* (fig. 5G and [supplementary table S32, Supplementary Material online](#)). Thus, the species-specific body coloration pattern (white head,

shoulders, and tail) of *T. leucocephalus* is most likely the result of a selective sweep on *EDNRB*, but other factors such as genetic drift and/or population bottlenecks might have contributed to the phenotype fixation as well, particularly as *T. leucocephalus* has a small population size.

## Discussion

### Physiological Adaptations

An increased blood  $\text{Ca}^{2+}$  concentration ( $\geq 2.6$  mmol/l) will result in a high calcium ion extracellular environment in tissues and is known to cause diseases in humans, such as hypercalcemia, atrioventricular block, and renal tubular damage (Pathy et al. 2005; Deakin et al. 2010; Minisola et al. 2015). Considering the significantly higher blood  $\text{Ca}^{2+}$  concentration in *T. francoisi* compared with other primates, it is reasonable to hypothesize that positively selected amino acid sites in *CACNA1C* and *CACNA1B*, coupled with mutations in five other PSGs (*CACNA1B*, *CD38*, *EGFR*, *HTR2B*, *ITPKB*, *MYLK*) in the KEGG pathway “calcium signaling” (table 1), regulate calcium entry into cells in limestone langurs as an adaptive mechanism (fig. 2A and D). As *CACNA1C* codes for the L-type voltage-gated calcium channel, which is the main entrance of calcium ions into cells with large conductance (Barad 2003; Lipp and Reither 2011), the substitution of *CACNA1C* plays a vital and direct role in regulating calcium entry (Liu et al. 2017; Ye et al. 2019). The *CACNA1C* gene codes for the  $\alpha_{1c}$  subunit of the  $\text{Ca}_v1.2$  channel and forms the tunnel body of  $\text{Ca}_v1.2$  (fig. 3H). The distal C-terminal domain of *CACNA1C* interacts with calmodulin, the  $\beta_2$  adrenergic receptor/cAMP/protein kinase ( $\beta_2\text{AR}$ -cAMP-PKA) signaling complex, calpain, and other proteins and regulates the calcium current in cells (Gao et al. 2001; Kim et al. 2004; Van Petegem et al. 2005; Catterall 2011). It has been reported that mutations R1906Q and Q1916R, which are close to the mutation found in limestone langurs (K1905R), lead to decreasing L-type calcium flux and cardiac disorders in humans (Liu et al. 2017; Ye et al. 2019). Consistently, our results revealed that K1905R of *CACNA1C* decreases the inward calcium flux into cells and inhibit the physiological stress of hypercalcemia compared with forest langurs and other primates (fig. 3H), and hence might be an adaptation to natural high  $\text{Ca}^{2+}$  intake. Additionally, *CACNA1C*, *CD38*, *EGFR*, and *MYLK* are also involved in the KEGG pathway of “oxytocin signaling.” Oxytocin stimulates an increase of intracellular calcium through the inward calcium current into cells and calcium release from the intracellular  $\text{Ca}^{2+}$  pool (Berrada et al. 2000; Lee et al. 2008), and it is quite reasonable that the PSGs in “ $\text{Ca}^{2+}$  signaling pathway” are also involved in “oxytocin signaling pathway” (supplementary fig. S11, Supplementary Material online). Moreover, the effects of positively selected amino acid sites in *CACNA1B* and other five PSGs (*CACNA1B*, *CD38*, *EGFR*, *HTR2B*, *ITPKB*, *MYLK*) in the KEGG pathway of “calcium signaling” should be examined through functional experiments in the future for a further understanding of the adaptive mechanism of limestone langurs.

Hypercalcemia in humans is known to cause heart damage, arrhythmia, arteriosclerosis, and high blood pressure (Warwick et al. 1961). Correspondingly, GO terms related to the circulatory system were also found to be overrepresented by PSGs in limestone langurs, including “vasoconstriction” (four genes), “blood circulation” (seven genes), “tonic smooth muscle contraction” (two genes), “regulation of blood vessel size” (four genes), and “regulation

of ventricular cardiac muscle cell action potential” (two genes) (all FDR adjusted  $P < 0.05$ , Fisher’s exact test; supplementary table S20, Supplementary Material online). It is reasonable to hypothesize that these PSGs found in all limestone langurs serve to stabilize the circulatory system in response to high blood  $\text{Ca}^{2+}$  concentrations. For example, *PKP2* also plays a vital role in the maintenance of blood pressure and heart rate, and loss-of-function mutations of *PKP2* cause arterial hypertension, heart disease, and sudden cardiac death (Pasquie et al. 2013; Ingles et al. 2018). Adaptive amino acid changes in these PSGs are consistent with the need to cope with the high blood  $\text{Ca}^{2+}$  concentration present in limestone langurs. Furthermore, the expanded orthologous gene families that are only found in all limestone langurs are also overrepresented in GO terms related to metal ion metabolism (supplementary table S25, Supplementary Material online). Additionally, the contracted orthologous gene families of “Myotubularin-like phosphatase” might also be related to the intracellular calcium homeostasis in limestone langurs (Romero-Suarez et al. 2010). The dysfunction of members in this gene family could decrease  $\text{Ca}^{2+}$  in the endoplasmic reticulum and inhibit  $\text{Ca}^{2+}$  entry into the cell (Weiss et al. 2009; Romero-Suarez et al. 2010). Thus, our findings clearly support adaptation of limestone langurs to a naturally high metal ion intake via food and water rich in metal ions (supplementary video 1, Supplementary Material online; Clements et al. 2006; Zhou et al. 2013).

### Morphological Adaptations

Interestingly, the GO terms of “limb morphogenesis” and “embryonic limb morphogenesis” were also enriched with two PSGs in all limestone langurs (*BBS2* and *TBC1D32*;  $P < 0.05$ , Fisher’s exact test; supplementary table S20, Supplementary Material online). *TBC1D32* is involved in the forelimb morphogenesis and mutations in *BBS2* are associated with Bardet–Biedl syndrome with skeletal deformity (Badano et al. 2003; Longatti et al. 2012). This selection signature is expected to be related to the different skeletal features between limestone and forest langurs. For example, the ratio of scapula width/height of limestone langurs is significantly higher compared with forest langurs (inhouse data;  $P < 0.001$ , Wilcoxon rank sum test; supplementary fig. S24, Supplementary Material online), which is consistent with increased joint flexibility and forelimb suspensory behavior in response to climbing on vertically oriented karst substrates (Püschel and Sellers 2016).

We also examined the possibility that the white and black pelage coloration of *T. leucocephalus* (white-headed langur) is the result of protective mimicry and an adaptation associated with living in a karst environment (fig. 5A; Huang 2011; Huang et al. 2016). All seven species of limestone langurs exhibit principally black fur coloration across their body, limbs, and head; thus, it is reasonable to regard this black fur coloration as ancestral for the group, and the white head, shoulders, and tail of *T. leucocephalus* to be a derived feature. *Trachypithecus francoisi* lives in evergreen broadleaf and limestone forest, and spends 60% of day time in trees and only 40% on rocks

(resting, traveling, and leaping). In contrast, *T. leucocephalus* lives mostly in typical limestone karst cliffs partly covered by plants and spends 71% of day time traveling and resting on rock surfaces (Mittermeier et al. 2013). Disruptive coloration is a type of camouflage in which a set of markings can create the appearance of false edges and boundaries that hinders the detection or recognition of an object's true outline and shape (Stevens and Merilaita 2011). As the head, shoulders, and tail of *T. leucocephalus* are white and hence similar to the karst rock surface (in *T. francoisi* the entire body is black except for a small patch of white on the cheeks), it is possible that the shape and outline of the monkeys are less easily detected when on a karst substrates. With our data, we have provided a potential explanation for differential adaptation of two species of limestone langurs to their subtle different habitat types. However, in the absence of additional study and confirmation, other explanations of the color pattern of *T. leucocephalus* (genetic drift and sexual selection) still remain because white hair color appears in forest langurs such as *T. germaini*. Additional work is required to fully understand the genomic mechanisms of pelage color variation in limestone langurs and their potential adaptations to different habitat types.

## Conclusion

Generating and analyzing the *T. francoisi* genome has provided comprehensive insights into the evolution of Asian langurs and identified genetic signatures related to their biology and evolution. Physiological and morphological adaptations of limestone langurs advance our knowledge of species differences and functional interactions between behavior, ecology, and the genome. For example, by comparing the genomes of limestone langurs and other primates, we identified mechanisms of adaptation to the challenges of living in harsh karst habitats. Functional assays further showed that a variant of CACNA1C (K1905R) attenuates the inward calcium current into the cell in vitro, indicating that limestone langurs have an enhanced ability to adapt to high calcium ion concentrations in the blood. The adaptation of limestone langurs to high blood calcium ion concentrations is conducive to further research into calcium metabolism (Schlingmann et al. 2016; Aihara et al. 2019). The consequences of other genomic changes in limestone langurs compared with forest langurs will need further verification through functional experiments in the future. With the availability of more genome assemblies, there is a substantial opportunity to use the naturally occurring functional variation to explore gene-environment interactions and the physiomorphological adaptive mechanisms of primates. Of the 504 primate species, >60%, among them many langur species, are highly threatened with extinction (Estrada et al. 2017). The population size reduction of many primate species and increased extinction risk represents an irreplaceable loss in genetic diversity. It highlights the urgency of a worldwide conservation effort for nonhuman primates, which contain inestimable value for scientific research, ecosystems health, and humanity.

## Materials and Methods

### Sampling and DNA Extraction

The blood sample used for de novo assembly and transcriptome analysis was obtained from one male individual of *T. francoisi* in the Wuzhou Langur Breeding Center, Guangxi Province, China, and DNA-extracted using the Genra Puregene Blood Kit (Qiagen). For the resequencing analysis, samples from nine langur species were used: François's langur (*T. francoisi*), white-headed langur (*T. leucocephalus*), Laos langur (*T. laotum*), Black langur (*T. ebenus*), and Hatinh langur (*T. hatinhensis*) as representatives of the *T. francoisi* or limestone langur group, Germain's langur (*T. germaini*) and East Javan langur (*T. auratus*) as representatives of the *T. cristatus* group, and Phayre's langur (*T. phayrei*) and Dusky langur (*T. obscurus*) as representatives of the *T. obscurus* group (supplementary fig. S1 and table S16, Supplementary Material online). Genomic DNA was extracted using the DNeasy Blood & Tissue Kit (Qiagen) and then used for followed sequencing.

### Genome Sequencing, De Novo Assembly, and Annotation of *T. francoisi*

Genomic DNA of a male *T. francoisi* was shared and multiple paired-end and mate-pair libraries were constructed with a size range of 180 bp to 15 kb (20 libraries; supplementary table S1, Supplementary Material online). All libraries were sequenced on the Illumina HiSeq 2500 platform. For raw reads, sequencing adaptors were removed; contaminated reads (chloroplast, mitochondrial, bacterial, and viral sequences) were screened by alignment to NCBI-NR database using BWA v0.7.13 (Li and Durbin 2009) with default parameters; polymerase chain reaction (PCR) duplicates were removed by FastUniq v1.1 (Xu et al. 2012). After filtering, a total of 598.37 Gb of data were retained for assembly according to the manufacturer's protocols. Furthermore, genomic DNA was sheared with a g-TUBE device (Covaris) with 20 kb settings and we generated 30.58 Gb sequence data using a PacBio SMRT sequencing platform. Additionally, 151.61 Gb clean Hi-C reads were obtained. In brief, we used the error correction module of Canu v1.5 (Koren et al. 2017) to complete PacBio subreads correction. The PacBio subreads were then assembled into contigs using WTDBG v1.1006 (<https://github.com/ruanjue/wtdbg>). Leveraging information from Illumina mate-pair reads, some contigs were linked using SSPACE v2.3 (Boetzer et al. 2011) and subsequently extended to longer contigs via the corrected PacBio subreads using PBjelly v14.9.9 (English et al. 2012). The iterative polishing of contigs was achieved by aligning Illumina paired-end reads using Pilon v1.22 (Walker et al. 2014). Finally, the raw assembly was corrected and clustered into 22 chromosome-level super-scaffolds (pseudochromosome, supplementary table S9, Supplementary Material online) with the aid of intrachromosome interaction signals generated by Hi-C technology (Burton et al. 2013). Total RNAs from multiple tissues were extracted using the Trizol reagent (Invitrogen, USA) followed by treatment with RNase-free DNase I (Promega, USA) according to the manufacturer's protocol. The RNA

sequencing library was constructed using an Illumina standard mRNA-Seq Prep Kit and sequenced on the Illumina 2500 platform. Protein-coding genes were predicted based on de novo, protein homology and RNA-seq approaches, respectively. A detailed description of genome size estimation, assembly, annotation, gene structure prediction, and functional annotation is included in the supplementary section 1, [Supplementary Material](#) online. The draft assembly was also evaluated using genome resequencing and transcriptomic data ([supplementary tables S6 and S10, Supplementary Material](#) online).

### Orthologous Gene Family and Phylogenetic Tree Construction

Orthologous gene families were constructed using a hierarchical clustering algorithm (hcluster\_sg) and TreeFam (Li et al. 2006). The phylogenetic tree was reconstructed using 10,280 single-copy genes shared by *T. francoisi* and 11 other primates (*H. sapiens*, *P. troglodytes*, *G. gorilla*, *M. mulatta*, *M. fascicularis*, *P. anubis*, *C. sabaesus*, *R. roxellana*, *R. bieti*, *C. jacchus*, and *O. garnettii*). The protein sequences of these single-copy genes were aligned by PRANK (Löytynoja and Goldman 2008), concatenated into a single supermatrix and back-translated to nucleotide sequences. A maximum-likelihood tree was reconstructed in RAxML software (version 8.0.19) (Stamatakis 2014) with 1,000 bootstrap iterations. Divergence times were estimated with mcmctree in PAML 4 (Yang 2007) based on 4-fold degenerate codon sites. We discarded the first 50,000 iterations as burn-in, and then ran the analysis for 200,000 iterations, sampling every two iterations. The rates at branches were set to autocorrelated. Convergence has been achieved by repeating the analysis ten times ([supplementary fig. S9, Supplementary Material](#) online), of which the two most consistent runs were used to calculate divergence times. The averages of the estimates of the two of most consistent runs were taken (Yang 2007). Calibration points used in Perelman et al. (2011) and Yu et al. (2016) were applied as normal priors to constrain the age of the following nodes: time to most recent common ancestor (TMRCA) of *Rhinopithecus*: 1.42 (1.05–1.79) Ma; TMRCA of *Homo-Pan*: 6.50 (6.00–7.00) Ma; TMRCA of Cercopithecoidea: 15.51 (14.46–16.56) Ma; TMRCA of Catarrhini: 29.00 (23.00–35.00) Ma; and TMRCA of Simiiformes: 43.00 (38.50–47.50) Ma (red cycled dots in [fig. 1B](#)). The expansion and contraction of orthologous gene families were determined by comparing the cluster size differences between the ancestor of *T. francoisi* and each of above-mentioned 11 primates ([supplementary tables S23 and S26, Supplementary Materials](#) online). To further identify expanded and contracted gene families before and after the divergence of limestone and forest langurs, the resequencing data of limestone and forest langurs were used to distinguish whether expansion and contraction of orthologous gene families occurred after or before the divergence of forest and limestone langurs ([supplementary section 2.4, Supplementary Materials](#) online). To avoid false determination of gene family expansions due to a fragmented assembly and annotation, we further extracted the full coding sequence

of different gene copies of candidate gene families in the genome of *T. francoisi* ([supplementary figs. S13 and S14, Supplementary Material](#) online).

### Identification of PSGs

PSGs were detected by estimating the ratio ( $\omega$ ) of nonsynonymous (dN) to synonymous (dS) substitutions in orthologous protein-coding sequences (Zhang et al. 2005). Orthologs among *T. francoisi* and 11 other primate species (*H. sapiens*, *P. troglodytes*, *G. gorilla*, *M. mulatta*, *M. fascicularis*, *P. anubis*, *C. sabaesus*, *R. roxellana*, *R. bieti*, *C. jacchus*, and *O. garnettii*) were obtained through multireciprocal BLAST. The longest transcript (all exons) of a specific gene was used to ensure that all protein isoforms are considered. A total of 10,280 orthologs were obtained and aligned using PRANK (Löytynoja and Goldman 2008). To reduce false positives generated by other type of errors, sequence regions of higher than expected nonsynonymous substitutions (a threshold of two or ten nonsynonymous substitutions in a window of 5 and 15 amino acids, respectively) along the *T. francoisi* branch were corrected by SWAMP (Harrison et al. 2014). The branch-site models of PAML were used to detect positive selection in *T. francoisi*. The nonsynonymous substitution caused by multinucleotide substitutions which was considered as errors during DNA replication were filtered by scripts. The  $\chi^2$  was used to compute *P* value and the FDR method was used to correct for multiple testing (*P* value < 0.01, FDR *P* < 0.05). The branch-site test of all the 10,280 orthologs were performed 3 times with different starting  $\omega$  values and candidate PSGs shared among the three runs were chosen as the PSGs in the *T. francoisi* genome. To further identify the PSGs specific to all five limestone langurs, we checked the positively selected substitutions (PSSs) in the herein studied five limestone langur and four forest langur species using the genome resequencing data. If the PSSs were only found in all five limestone langur species but not in forest langurs, these PSSs were regarded to occur in the common ancestor of the limestone langurs, and PSGs with these PSSs are regarded as putative targets of positive selection specific to limestone langurs ([supplementary fig. S10, Supplementary Material](#) online). Functional classification and enrichment analyses were performed using KOBAS 3.0 (Xie et al. 2011).

### Two-Electrode Voltage-Clamp Analysis of CACNA1C in *Xenopus laevis* Oocytes

For whole-cell current recordings of the transmembrane calcium channel in *Xenopus laevis* oocytes, the cDNA of CACNA1C and CACNA1C-K1905R were cloned into the pGEMHE oocyte expression vector. Capped RNA (cRNA) synthesized from the linearized pGEMHE vector DNA templates were injected into each oocyte. After 2 days incubation in ND96 solution (96 mM NaCl, 2 mM KCl, 1 mM MgCl<sub>2</sub>, 1.8 mM CaCl<sub>2</sub>, 10 mM HEPES/NaOH, pH 7.4) supplemented with 25  $\mu\text{g l}^{-1}$  gentamycin at 18 °C, oocytes were voltage-clamped with a TEV 200 A amplifier (Dagan Corporation) and monitored by computer through Digidata 1440 A/D converter and pCLAMP 10.4 software (Axon Instruments). For comparative analysis of CACNA1C and its mutant, 10 mM

CaCl<sub>2</sub> were added to the bath solution (supplementary fig. S16, Supplementary Material online). Oocytes were harvested at stage V to VI from at least five *Xenopus* and maintained in ND96 solution overnight prior to injections. For each experiment, ten oocytes were recorded. All data are presented as mean ± SD.

### Lentiviral Transfection and Cell Culture

The constructed recombinant shuttle plasmid pCDH-pMD2.G-psPAX-copGFP (CACNA1C and CACNA1C-K1905R) and lentivirus via lipofectamine 3000 helper plasmid were cotransfected into HEK293FT cells to produce virus. Then, we used the virus to infect HEK293FT cells to obtain CACNA1C and CACNA1C-K1905R cells. After detecting and screening via flow cytometer, cultured cells were used for qPCR, Western blots, and calcium imaging.

### Quantitative Real-Time PCR

Total RNA was extracted from HEK293FT, CACNA1C, and CACNA1C-K1905R cells. We amplified fragments of CACNA1C and an internal control gene named cyclophilin, which is commonly used in human HEK293FT cells, using Cyclophilin (5'-CCGAGGAAAACCGTGTACTATTAG-3', 5'-TGCTGTCTTTGGGACCTTG-3') and Assay3 primers (5'-TCCAAGACACGGCAAACA-3' and 5'-GTTGAAGAGGGACACGAAGTAG-3'). Amplification was performed with a LineGene 9600 Plus thermocycler (Bioer Technology) using a 2 min 95 °C initial denaturation, 40 cycles of 95 °C for 15 s and 60 °C for 1 min. We analyzed qPCR data using the auto-threshold (CT) method, setting the threshold fluorescence (Rn) to 0.05 (fig. 3D).

### Immunofluorescence Technique (Western Blotting)

Immunoblot analysis was performed according to standard protocols. Proteins were separated by SDS-PAGE, transferred to nitrocellulose membrane, blocked in skim milk in TBST, incubated with primary antibodies overnight at 4 °C, and incubated with secondary antibodies conjugated with HRP. Primary antibodies used in this study are anti-CACNA1C (Cat. No. ab84814, Abcam Company, England) and β-actin (Cat. No. MD2142 and Cat. No. MD2141, EPSILON, China) (fig. 3E and F and supplementary fig. S17, Supplementary Material online).

### Cytosolic Ca<sup>2+</sup> Concentration Measurements

To detect changes in intracellular calcium concentration, HEK293FT cells with CACNA1C and CACNA1C-K1905R were cultured in 3-cm cell plates with a coverslip. All cells were loaded with Fura2-AM (Cat. No. F025, Dojindo Company, China). For Ca<sup>2+</sup> imaging, cells were excited by 340 and 380 nm UV light (Lambda DG-4, SUTTER) using a Fura-2 dichroic filter cube and visualized by water immersion objective lens (Nikon MODEL ECLIPSE FN1, Eclipse Ti) in Ca<sup>2+</sup> free medium (Tang et al. 2003; Wang et al. 2016). After 3 min of observation, the medium was increased to 3.5 mM Ca<sup>2+</sup> with a peristaltic pump. Throughout the process, the emitted light was collected by a microscope charge coupled device (ANDOR iXon3 EMOOD) and the images

were digitized by CellVision (Version 1.3) software (supplementary figs. S18 and S19, Supplementary Material online).

### Genome Resequencing, Phylogenetics, and Population Structure Analyses of Langurs

Whole-genome resequencing data for 23 individuals of nine langur species was generated using the Illumina Hiseq 4000 platform with high coverage (mean 31.59×, range 23.93–45.02×). Reads from the 23 resequenced langurs were aligned to the reference langur genome using BWA (Li and Durbin 2009). We performed SNP calling using the best practices in GATK (McKenna et al. 2010) with the details provided in the Supplementary Material online. A phylogenetic tree based on autosomal SNPs was inferred using the neighborhood-joining method as implemented in TreeBest software (Ruan et al. 2007) with 1,000 bootstrap iterations, with *R. roxellana* as outgroup (supplementary fig. S20, Supplementary Material online). Divergence time estimation was conducted with mcmctree of PAML 4 (Yang 2007) using the HKY85 substitution model and rates set to auto-correlated. We discarded the first 50,000 iterations as burn-in, and then ran the analysis for 200,000 iterations, sampling every two iterations. Convergence has been achieved by repeating the analysis ten times (supplementary fig. S21, Supplementary Material online), of which the two most consistent runs were used to calculate divergence times. The averages of the estimates of the two of most consistent runs were taken (Yang 2007). We used the split between *Rhinopithecus* and *Trachypithecus* as a calibration point (9.30 ± 3.30 Ma). Additionally, TMRCA of *T. obscurus* and *T. phayrei*: 1.20 (0.65–1.72) Ma, TMRCA of *T. auratus* and *T. germaini*: 0.80 (0.33–1.27) Ma and TMRCA of *T. obscurus* and *T. auratus*: 2.45 (1.69–3.23) Ma were also set as calibration points (Perelman et al. 2011; Roos et al. 2019). Genetic structure of *T. francoisi* and *T. leucocephalus* was inferred using the program *frappe* v1.1 (Tang et al. 2005). We predefined the number of genetic clusters *K* from 2 to 4. The maximum iteration of the expectation-maximization algorithm was set to 10,000. The PCA of eight *T. francoisi* and eight *T. leucocephalus* individuals as well as for all langurs was conducted using EIGENSOFT (version 7.2.1) (Price et al. 2006) and the significance of eigenvectors was determined with the Tracy–Widom test in EIGENSOFT. Linkage disequilibrium for *T. francoisi* and *T. leucocephalus* was calculated using the haploview software (Barrett et al. 2005) with the max distance set as 500 kb (supplementary fig. S22, Supplementary Material online).

### Demographic History Reconstruction

Changes in effective population size for each one individual of the nine langur species were inferred from a haploid pairwise sequentially Markovian coalescence (PSMC) model (Li and Durbin 2011) with parameters “-g 10 -R -u 1.0e-8 -N 25 -t 15 -r 5 -p '4 + 25\*2 + 4 + 6'”. The unit of estimated TMRCA is 2 *N*<sub>0</sub> time; the mean generation time was set at 10 years and μ (unit: bp/generation) was set to 1.0 × 10<sup>-8</sup> according to a previous study (Xue et al. 2016).

## Selective Signal in *T. leucocephalus* Compared with *T. francoisi*

The genetic differentiation of *T. leucocephalus* and *T. francoisi* was calculated by pairwise  $F_{ST}$  (Weir and Cockerham 1984) and the polymorphism levels in both species were quantified by pairwise nucleotide diversity ( $\theta_\pi$ ) (Tajima 1983), using a sliding-window approach (50 kb windows with 25 kb increments). The  $F_{ST}$  values were Z-transformed (Axelsson et al. 2013; Yang et al. 2016), and the  $\theta_\pi$  ratios (*T. leucocephalus*/*T. francoisi*) were  $\log_2$ -transformed (Qiu et al. 2015). We considered the windows with the top 5% values for the  $Z(F_{ST})$  and  $\log_2(\theta_\pi)$  ratios) simultaneously as the candidate outliers under strong selective sweep. All the outlier windows were assigned to corresponding genes. Furthermore, we estimated the cross-population extended haplotype homozygosity (XP-EHH; Sabeti et al. 2007) statistic for *T. leucocephalus*, using the control group (*T. francoisi*) as a reference and applying the top 5th percentile outliers as threshold to identify candidate genes. The number of overlapping candidate genes among the  $F_{ST}$ ,  $\theta_\pi$  ratio, and XP-EHH analyses were chosen as the genes under selective sweep in *T. leucocephalus* (supplementary table S30, Supplementary Material online).

## RNA Sequencing

Total RNA was isolated from tail hair follicles of three *T. leucocephalus* and three *T. francoisi* individuals. Sequencing libraries were constructed using an Illumina standard mRNA-Seq Prep Kit. The libraries were sequenced on an Illumina HiSeq platform and 150-bp paired-end reads were generated. Transcriptome reads were mapped to the langur genome using TopHat and Bowtie 2 (Trapnell et al. 2009; Langmead and Salzberg 2012).

## Supplementary Material

Supplementary data are available at *Molecular Biology and Evolution* online.

## Acknowledgments

The project was supported by Strategic Priority Research Program of the Chinese Academy of Sciences (XDB31000000), the National Natural Science Foundation of China (31761133020, 31970390, 31821001, 31772438), and National Key R&D Program of China (2016YFC0503200). The authors thank Meng Yao, Jiang Zhou, Tao Meng, and Qihai Zhou for their help with sampling, and Tieshan Tang, Paul Garber, Wang Tian, Meng Dong, Zhenxin Fan, Fenghua Lv, Chuanyun Li, Qiaoqiao He, Lin Yang, Quan Kang, and Qi Wu for assistance with data analyses. They are grateful to the editors and anonymous reviewers for their insightful and constructive feedback.

## Author Contributions

M.L., Z.L., and C.R. conceived and designed the project. Z.L., L.Z., Z.Y., Z.R., and F.H. managed the project. T.Q., C.T., Y.L., S.W., and J.W. collected samples. Z.L. coordinated genome assembly, annotation, and bioinformatics analyses. F.H., L.Z.,

and Z.Y. performed genome assembly and annotation. Z.Y., L.Z., X.T., F.D., Y.X., Z.Y., and F.H. performed genetic analyses. Z.R. and Z.X. implemented the point mutation and TEVC experiment. L.L., Z.W., and C.H. discussed the data. Z.L., L.Z., Z.Y., Z.R., and F.H. wrote the article with contributions from M.L., C.H., C.R., L.L., S.W., and J.W. All authors contributed to data interpretation.

## References

- Aihara S, Yamada S, Oka H, Kamimura T, Nakano T, Tsuruya K, Harada A. 2019. Hypercalcemia and acute kidney injury induced by eldcalcitol in patients with osteoporosis: a case series of 32 patients at a single facility. *Ren Fail.* 41(1):88–97.
- Axelsson E, Ratnakumar A, Arendt ML, Maqbool K, Webster MT, Perloski M, Liberg O, Arnemo JM, Hedhammar A, Lindblad-Toh K. 2013. The genomic signature of dog domestication reveals adaptation to a starch-rich diet. *Nature* 495(7441):360–364.
- Badano JL, Kim JC, Hoskins BE, Lewis RA, Ansley SJ, Cutler DJ, Castellan C, Beales PL, Leroux MR, Katsanis N. 2003. Heterozygous mutations in *BBS1*, *BBS2* and *BBS6* have a potential epistatic effect on Bardet-Biedl patients with two mutations at a second *BBS* locus. *Hum Mol Genet.* 12(14):1651–1659.
- Bäder S, Glaubke E, Grüb S, Muhs S, Wellbrock J, Nalaskowski M, Lange T, Windhorst S. 2018. Effect of the actin- and calcium-regulating activities of ITPKB on the metastatic potential of lung cancer cells. *Biochem J.* 475(12):2057–2071.
- Barad M. 2003. Later developments: molecular keys to age-related memory impairment. *Alzheimer Dis Assoc Dis.* 17(3):168–176.
- Barrett JC, Fry B, Maller J, Daly MJ. 2005. Haploview: analysis and visualization of LD and haplotype maps. *Bioinformatics* 21(2):263–265.
- Beall CM. 2006. Andean, Tibetan, and Ethiopian patterns of adaptation to high-altitude hypoxia. *Integr Comp Biol.* 46(1):18–24.
- Berrada K, Plesnicher CL, Luo X, Thibonnier M. 2000. Dynamic interaction of human vasopressin/oxytocin receptor subtypes with G protein-coupled receptor kinases and protein kinase C after agonist stimulation. *J Biol Chem.* 275(35):27229–27237.
- Boetzer M, Henkel CV, Jansen HJ, Butler D, Pirovano W. 2011. Scaffolding pre-assembled contigs using SSPACE. *Bioinformatics* 27(4):578–579.
- Burton JN, Adey A, Patwardhan RP, Qiu R, Kitzman JO, Shendure J. 2013. Chromosome-scale scaffolding of *de novo* genome assemblies based on chromatin interactions. *Nat Biotechnol.* 31(12):1119–1125.
- Carbone L, Harris RA, Gnerre S, Veeramah KR, Lorente-Galdos B, Huddleston J, Meyer TJ, Herrero J, Roos C, Aken B, et al. 2014. Gibbon genome and the fast karyotype evolution of small apes. *Nature* 513(7517):195–201.
- Catterall WA. 2011. Voltage-gated calcium channels. *Cold Spring Harb Perspect Biol.* 3:1–23.
- Clapham DE. 2007. Calcium signaling. *Cell* 131(6):1047–1058.
- Clements R, Sodhi NS, Schilthuizen M, Ng P. 2006. Limestone karsts of Southeast Asia: imperiled arks of biodiversity. *BioScience* 56(9):733–742.
- Deakin CD, Nolan JP, Sunde K, Koster RW. 2010. European Resuscitation Council Guidelines for Resuscitation 2010 Section 3. Electrical therapies: automated external defibrillators, defibrillation, cardioversion and pacing. *Resuscitation* 81(10):1293–1304.
- Deng L, Xu S. 2017. Adaptation of human skin color in various populations. *Hereditas* 155(1):
- English AC, Richards S, Han Y, Wang M, Vee V, Qu J, Qin X, Muzny DM, Reid JG, Worley KC, et al. 2012. Mind the gap: upgrading genomes with Pacific Biosciences RS long-read sequencing technology. *PLoS One* 7(11):e47768.
- Estrada A, Garber PA, Rylands AB, Roos C, Fernandez-Duque E, Di Fiore A, Nekaris KA-I, Nijman V, Heymann EW, Lambert JE, et al. 2017. Impending extinction crisis of the world's primates: why primates matter. *Sci Adv.* 3(1):e1600946.
- Ford D, Williams PW. 2007. Karst hydrogeology and geomorphology. New York: Wiley.

- Fumagalli M, Moltke I, Grarup N, Racimo F, Bjerregaard P, Jørgensen ME, Korneliussen TS, Gerbault P, Skotte L, Linneberg A, et al. 2015. Greenlandic Inuit show genetic signatures of diet and climate adaptation. *Science* 349(6254):1343–1347.
- Gao T, Cuadra AE, Ma H, Bünemann M, Gerhardtstein BL, Cheng T, Ten Eick R, Hosey MM. 2001. C-terminal fragments of the  $\alpha_{1C}$  ( $Ca_v1.2$ ) subunit associate with and regulate L-type calcium channels containing C-terminal-truncated  $\alpha_{1C}$  subunits. *J Biol Chem* 276(24):21089–21097.
- Garipey CE, Cass DT, Yanagisawa M. 1996. Null mutation of endothelin receptor type B gene in spotting lethal rats causes aganglionic megacolon and white coat color. *Proc Natl Acad Sci U S A* 93(2):867–872.
- Groves C. 2001. Primate taxonomy. Washington (DC): Smithsonian Institution Press.
- Hao Z, Kuang YW, Kang M. 2015. Untangling the influence of phylogeny, soil and climate on leaf element concentrations in a biodiversity hotspot. *Funct Ecol* 29(2):165–176.
- Harrison PW, Jordan GE, Montgomery SH. 2014. SWAMP: sliding window alignment masker for PAML. *Evol Bioinform Online* 10:197–204.
- Heyes S, Pratt WS, Rees E, Dahimene S, Ferron L, Owen MJ, Dolphin AC. 2015. Genetic disruption of voltage-gated calcium channels in psychiatric and neurological disorders. *Prog Neurobiol* 134:36–54.
- Hosoda K, Hammer RE, Richardson JA, Baynash AG, Cheung JC, Giaid A, Yanagisawa M. 1994. Targeted and natural (piebald-lethal) mutations of endothelin-B receptor gene produce megacolon associated with spotted coat color in mice. *Cell* 79(7):1267–1276.
- Hu G. 2007. Socioecology and behavioural flexibility of Francois' langur (*Trachypithecus francoisi*) in Mayanghe Nature Reserve, Southwest China [PhD thesis]. Canberra (ACT): The Australian University.
- Huang CM. 2011. Exploring the secret of karst fairy. Nanjing (China): Jiangsu Science & Technology Press.
- Huang CM, Li YB. 2005. How does the white-headed langur (*Trachypithecus leucocephalus*) adapt locomotor behavior to its unique limestone hill habitat? *Primates* 46(4):261–267.
- Huang CM, Li YB, Zhou QH. 2016. Emphasis on white-headed langur adaptation to karst environment. *B Biol* 51:1–4.
- Huang CM, Wu H, Zhou QH, Li YB, Cai XW. 2008. Feeding strategy of Francois' langur and white-headed langur at Fusui, China. *Am J Primatol* 70(4):320–326.
- Ilardo MA, Moltke I, Korneliussen TS, Cheng J, Stern AJ, Racimo F, de Barros Damgaard P, Sikora M, Seguin-Orlando A, Rasmussen S, et al. 2018. Physiological and genetic adaptations to diving in sea nomads. *Cell* 173(3):569–580.
- Ingles J, Bagnall RD, Yeates L, McGrady M, Berman Y, Whalley D, Dufloy J, Semsarian C. 2018. PKP2 loss-of-function variants in probands with sudden unexplained cardiac death events. *Circulation* 138:A13371.
- Ji FT, Li N, Deng X. 2009. Calcium contents and high calcium adaptation of plants in karst areas of China. *Chin J Plant Ecol* 33:926–935.
- Jin WW, Long Y, Fu CH, Zhang LB, Xiang J, Wang BS, Li MT. 2018.  $Ca^{2+}$  imaging and gene expression profiling of *Lonicera Confusa* in response to calcium-rich environment. *Sci Rep* 8(1):7068.
- Kim J, Ghosh S, Nunziato DA, Pitt GS. 2004. Identification of the components controlling inactivation of voltage-gated  $Ca^{2+}$  channels. *Neuron* 41(5):745–754.
- Koren S, Walenz BP, Berlin K, Miller JR, Bergman NH, Phillippy AM. 2017. Canu: scalable and accurate long-read assembly via adaptive *k*-mer weighting and repeat separation. *Genome Res* 27(5):722–736.
- Langmead B, Salzberg SL. 2012. Fast gapped-read alignment with Bowtie 2. *Nat Methods* 9(4):357–359.
- Lee ES, Uhm KO, Lee YM, Kwon J, Park SH, Soo KH. 2008. Oxytocin stimulates glucose uptake in skeletal muscle cells through the calcium-CaMKK-AMPK pathway. *Regul Pept* 151(1–3):71–75.
- Lek M, Karczewski KJ, Minikel EV, Samocha KE, Banks E, Fennell T, O'Donnell-Luria AH, Ware JS, Hill AJ, Cummings BB, et al. 2016. Analysis of protein-coding genetic variation in 60,706 humans. *Nature* 536(7616):285–291.
- Li H, Coghlan A, Ruan J, Coin LJ, Hériché JK, Osmotherly L, Li RQ, Liu T, Zhang Z, Bolund L, et al. 2006. TreeFam: a curated database of phylogenetic trees of animal gene families. *Nucleic Acids Res* 34(90001):D572–D580.
- Li H, Durbin R. 2009. Fast and accurate short read alignment with Burrows–Wheeler transform. *Bioinformatics* 25(14):1754–1760.
- Li H, Durbin R. 2011. Inference of human population history from individual whole-genome sequences. *Nature* 475(7357):493–496.
- Li ZY, Wei Y, Rogers E. 2003. Food choice of white-headed langurs in Fusui, China. *Int J Primatol* 24(6):1189–1205.
- Lipp P, Reither G. 2011. Protein kinase C: the “masters” of calcium and lipid. *Cold Spring Harb Perspect Biol* 3(7):a004556.
- Liu X, Shen Y, Xie J, Bao H, Cao Q, Wan R, Xu X, Zhou H, Huang L, Xu Z, et al. 2017. A mutation in the CACNA1C gene leads to early repolarization syndrome with incomplete penetrance: a Chinese family study. *PLoS One* 12(5):e0177532.
- Liu X, Wu Q, Huang Z, Huang C, Zhou Q. 2016. Nutritional content of dry season foods and its influences on food choice of Francois' langurs at Nonggang. *Acta Ther Sin* 36:241–247.
- Longatti A, Lamb CA, Razi M, Yoshimura S-I, Barr FA, Tooze SA. 2012. TBC1D14 regulates autophagosome formation via Rab11- and ULK1-positive recycling endosomes. *J Cell Biol* 197(5):659–675.
- Löytynoja A, Goldman N. 2008. Phylogeny-aware gap placement prevents errors in sequence alignment and evolutionary analysis. *Science* 320:1632–1635.
- Luo XQ, Wang CY, Yang HY, Liao XR. 2012. Studies on adaptive mechanisms of karst dominant plant species to drought and high calcium stress. *Chin Agric Bull* 28:1–5.
- Mattle-Greminger MP, Bilgin Sonay T, Nater A, Pybus M, Desai T, de Valles G, Casals F, Scally A, Bertranpetit J, Marques-Bonet T, et al. 2018. Genomes reveal marked differences in the adaptive evolution between orangutan species. *Genome Biol* 19(1):193.
- McKenna A, Hanna M, Banks E, Sivachenko A, Cibulskis K, Kernysky A, Garimella K, Altshuler D, Gabriel S, Daly M, et al. 2010. The Genome Analysis Toolkit: a MapReduce framework for analyzing next-generation DNA sequencing data. *Genome Res* 20(9):1297–1303.
- Metallinos DL, Bowling AT, Rine J. 1998. A missense mutation in the endothelin-B receptor gene is associated with Lethal White Foal Syndrome: an equine version of Hirschsprung disease. *Mamm Genome* 9:426–431.
- Minisola S, Pepe J, Piemonte S, Cipriani C. 2015. The diagnosis and management of hypercalcaemia. *BMJ* 350(Jun 02):h2723–h2723.
- Minton K. 2014. Coordinating calcium signaling. *Nat Rev Mol Cell Biol* 15(3):152–152.
- Mittermeier RA, Rylands AB, Wilson DE. 2013. Handbook of mammals of the world: primates. Barcelona (Spain): Lynx Edicions.
- Miwa M, Inoue-Murayama M, Aoki H, Kunisada T, Hiragaki T, Mizutani M, Ito S. 2007. Endothelin receptor B2 (*EDNRB2*) is associated with the panda plumage colour mutation in Japanese quail. *Anim Genet* 38(2):103–108.
- Osterholz M, Walter L, Roos C. 2008. Phylogenetic position of the langur genera *Semnopithecus* and *Trachypithecus* among Asian colobines, and genus affiliations of their species groups. *BMC Evol Biol* 8:58.
- Palesch D, Bosinger SE, Tharp GK, Vanderford TH, Paiardini M, Chahroudi A, Johnson ZP, Kirchoff F, Hahn BH, Norgren RB, et al. 2018. Sooty mangabey genome sequence provides insight into AIDS resistance in a natural SIV host. *Nature* 553(7686):77–81.
- Pasquie JL, Hedon C, Alfalasi O, Thomann S, Massin F, Cransac F, Cung TT, Davy JM. 2013. Endurance sports precipitate phenotypic expression of arrhythmogenic right ventricular cardiomyopathy (ARVC) in asymptomatic PKP2-mutation carriers. *Eur Heart J* 34(Suppl 1):1901.
- Pathy J, Sinclair AJ, Morley JE. 2005. Principles and practice of geriatric medicine. Vol. 2. 4th ed. Hoboken: John Wiley & Sons.
- Pearson K. 1901. On lines and planes of closest fit to system of points in space. *Philos Mag B* 11:559–572.
- Perelman P, Johnson WE, Roos C, Seuánez HN, Horvath JE, Moreira MA, Kessing B, Pontius J, Roelke M, Rumpler Y, et al. 2011. A molecular phylogeny of living primates. *PLoS Genet* 7(3):e1001342.

- Plumbly W, Brandon N, Deeb TZ, Hall J, Harwood AJ. 2019. L-type voltage-gated calcium channel regulation of *in vitro* human cortical neuronal networks. *Sci Rep*. 9(1):13810.
- Price AL, Patterson NJ, Plenge RM, Weinblatt ME, Shadick NA, Reich D. 2006. Principal components analysis corrects for stratification in genome-wide association studies. *Nat Genet*. 38(8):904–909.
- Puffenberger EG, Hosoda K, Washington SS, Nakao K, deWit D, Yanagisawa M, Chakravarti A. 1994. A missense mutation of the endothelin-B receptor gene in multigenic Hirschsprung's disease. *Cell* 79(7):1257–1266.
- Püschel TA, Sellers WI. 2016. Standing on the shoulders of apes: analyzing the form and function of the hominoid scapula using geometric morphometrics and finite element analysis. *Am J Phys Anthropol*. 159(2):325–341.
- Qian H, Patriarchi T, Price JL, Matt L, Lee B, Nieves-Cintrón M, Buonarali OR, Chowdhury D, Nanou E, Nystoriak MA, et al. 2017. Phosphorylation of Ser<sup>1928</sup> mediates the enhanced activity of the L-type Ca<sup>2+</sup> channel Cav1.2 by the  $\beta$ 2-adrenergic receptor in neurons. *Sci Signal*. 10:aaf9659.
- Qiu Q, Wang LZ, Wang K, Yang YZ, Ma T, Wang ZF, Zhang X, Ni ZQ, Hou FJ, Long RJ, et al. 2015. Yak whole-genome resequencing reveals domestication signatures and prehistoric population expansions. *Nat Commun*. 6(1):10283.
- Romero-Suarez S, Shen J, Brotto L, Hall T, Mo C, Valdivia HH, Andresen J, Wacker M, Nosek TM, Qu C, Brotto M. 2010. Muscle-specific inositolide phosphatase (MIP/MTMR14) is reduced with age and its loss accelerates skeletal muscle aging process by altering calcium homeostasis. *Aging* 2(8):504–513.
- Roos C, Liedigk R, Thinh V, Nadler T, Zinner D. 2019. The hybrid origin of the Indochinese gray langur *Trachypithecus crepusculus*. *Int J Primatol*. 40(1):9–27.
- Rowe N, Myers M. 2016. All the world's primates. Charlestown (RI): Pogonias Press.
- Ruan J, Li H, Chen ZZ, Coghlan A, Coin LJM, Guo YR, Hériché JK, Hu Y, Kristiansen K, Li RQ, et al. 2007. TreeFam: 2008 update. *Nucleic Acids Res*. 36(Database):D735–D740.
- Sabeti PC, Varilly P, Fry B, Lohmueller J, Hostetter E, Cotsapas C, Xie X, Byrne EH, McCarroll SA, Gaudet R, et al. 2007. Genome-wide detection and characterization of positive selection in human populations. *Nature* 449(7164):913–918.
- Scheinfeldt LB, Tishkoff SA. 2013. Recent human adaptation: genomic approaches, interpretation and insights. *Nat Rev Genet*. 14(10):692–702.
- Schlingmann KP, Ruminska J, Kaufmann M, Dursun I, Patti M, Kranz B, Pronicka E, Ciara E, Akcay T, Bulus D, et al. 2016. Autosomal-recessive mutations in *SLC34A1* encoding sodium-phosphate cotransporter 2A cause idiopathic infantile hypercalcemia. *J Am Soc Nephrol*. 27:604–614.
- Schmitz J, Noll A, Raabe CA, Churakov G, Voss R, Kiefmann M, Rozhdestvensky T, Brosius T, Baertsch R, Clawson H, et al. 2016. Genome sequence of the basal haplorhine primate *Tarsius syrichta* reveals unusual insertions. *Nat Commun*. 7(1):12997.
- Stamatakis A. 2014. RAxML Version 8: a tool for phylogenetic analysis and post-analysis of large phylogenies. *Bioinformatics* 30(9):1312–1313.
- Stevens M, Merilaita S. 2011. Animal camouflage: function and mechanisms. In: Stevens M, Merilaita S, editors. Animal camouflage: mechanisms and functions. Cambridge: Cambridge University Press. p. 1–16.
- Tajima F. 1983. Evolutionary relationship of DNA sequences in finite populations. *Genetics* 105(2):437–460.
- Tang H, Peng J, Wang P, Risch NJ. 2005. Estimation of individual admixture: analytical and study design considerations. *Genet Epidemiol*. 28(4):289–301.
- Tang TS, Tu H, Chan EY, Maximov A, Wang Z, Wellington CL, Hayden MR, Bezprozvanny I. 2003. Huntingtin and huntingtin-associated protein 1 influence neuronal calcium signaling mediated by inositol-(1,4,5) triphosphate receptor type 1. *Neuron* 39(2):227–239.
- Teare J. 2002. International species information system physiological data reference values. Apple Valley (MN): International Species Information System.
- Trapnell C, Pachter L, Salzberg SL. 2009. TopHat: discovering splice junctions with RNA-Seq. *Bioinformatics* 25(9):1105–1111.
- Van Petegem F, Chatelain FC, Minor DL Jr. 2005. Insights into voltage-gated calcium channel regulation from the structure of the Cav1.2 IQ domain-Ca<sup>2+</sup>/calmodulin complex. *Nat Struct Mol Biol*. 12(12):1108–1115.
- Walker BJ, Abeel T, Shea T, Priest M, Abouelliel A, Sakthikumar S, Cuomo CA, Zeng Q, Wortman J, Young SK, et al. 2014. Pilon: an integrated tool for comprehensive microbial variant detection and genome assembly improvement. *PLoS One* 9(11):e112963.
- Wang QC, Zheng QX, Tan HY, Zhang B, Li XL, Yang YX, Yu J, Liu Y, Chai H, Wang X, et al. 2016. TMCO1 is an ER Ca<sup>2+</sup> load-activated Ca<sup>2+</sup> channel. *Cell* 165(6):1454–1466.
- Wang Y, Liu Z, Ai Y, Zhang L, Zou Y, Peng Q. 2017. Blocking the CD38/cADPR pathway plays a double-edged role in LPS stimulated microglia. *Neuroscience* 361:34–42.
- Warwick OH, Yendt ER, Olin JS. 1961. The clinical features of hypercalcemia associated with malignant disease. *Can Med Assoc J*. 85:719–723.
- Weir BS, Cockerham CC. 1984. Estimating F-statistics for the analysis of population structure. *Evolution* 38:1358–1370.
- Weiss N, Qusairi L, Bergbey C, Allard B, Mandel J, Laporte J, Buj-Bello A, Jacquemond V. 2009. Impaired sarcoplasmic reticulum calcium release in skeletal muscle fibers from myotubularin-deficient mice. *Biophys J*. 3:10a.
- Winder SJ, Walsh MP. 1993. Calponin: thin filament-linked regulation of smooth muscle contraction. *Cell Signal*. 5(6):677–686.
- Workman C. 2010. Diet of the Delacour's langur (*Trachypithecus delacouri*) in Van Long Nature Reserve, Vietnam. *Am J Primatol*. 72:317–324.
- Workman C, Dung L. 2009. The chemistry of eaten and uneaten leaves by Delacour's langurs (*Trachypithecus delacouri*) in Van Long Nature Reserve, Vietnam. *Viet J Primatol*. 3:29–36.
- Wu G, Li MT, Zhong FX, Fu CH, Sun J, Yu LJ. 2011. *Lonicera confusa* has an anatomical mechanism to respond to calcium-rich environment. *Plant Soil*. 338(1–2):343–353.
- Xie C, Mao XZ, Huang JJ, Ding Y, Wu JM, Dong S, Kong L, Gao G, Li CY, Wei LP. 2011. KOBAS 2.0: a web server for annotation and identification of enriched pathways and diseases. *Nucleic Acids Res*. 39(suppl\_2):W316–W322.
- Xu HB, Luo X, Qian J, Pang XH, Song JY, Qian GR, Chen JH, Chen SL. 2012. FastUniq: a fast de novo duplicates removal tool for paired short reads. *PLoS One* 7(12):e52249.
- Xue C, Raveendran M, Harris RA, Fawcett GL, Liu X, White S, Dahdoui M, Rio Deiros D, Below JE, Salerno W, et al. 2016. The population genomics of rhesus macaques (*Macaca mulatta*) based on whole-genome sequences. *Genome Res*. 26(12):1651–1662.
- Yang J, Li WR, Lv FH, He SG, Tian SL, Peng WF, Sun YW, Zhao YX, Tu XL, Zhang M, et al. 2016. Whole-genome sequencing of native sheep provides insights into rapid adaptations to extreme environments. *Mol Biol Evol*. 33(10):2576–2592.
- Yang ZH. 2007. PAML 4: phylogenetic analysis by maximum likelihood. *Mol Biol Evol*. 24(8):1586–1591.
- Ye D, Tester DJ, Zhou W, Papagiannis J, Ackerman MJ. 2019. A pore-localizing CACNA1C-E1115K missense mutation, identified in a patient with idiopathic QT prolongation, bradycardia, and autism spectrum disorder, converts the L-type calcium channel into a hybrid nonselective monovalent cation channel. *Heart Rhythm* 16(2):270–278.
- Yoshihara M, Sato T, Saito D, Ohara O, Kuramoto T, Suyama M. 2017. A deletion in the intergenic region upstream of *Ednrb* causes head spot in the rat strain KFRS4/Kyo. *BMC Genet*. 18(1):29.
- Yu L, Wang GD, Ruan J, Chen YB, Yang CP, Cao X, Wu H, Liu YH, Du ZL, Wang XP, et al. 2016. Genomic analysis of snub-nosed monkeys (*Rhinopithecus*) identifies genes and processes related to high-altitude adaptation. *Nat Genet*. 48(8):947–952.

- Zhang JZ, Nielsen R, Yang ZH. 2005. Evaluation of an improved branch-site likelihood method for detecting positive selection at the molecular level. *Mol Biol Evol.* 22(12): 2472–2479.
- Zheng BX, Xu QQ, Shen YP. 2002. The relationship between climate change and Quaternary glacial cycles on the Qinghai–Tibetan Plateau: review and speculation. *Quat Int.* 97:93–101.
- Zhou Q, Tang Z, Li Y, Huang C. 2013. Food diversity and choice of white-headed langur in fragmented limestone hill habitat in Guangxi, China. *Acta Ecol Sin.* 33(2):109–113.
- Zhou QH, Huang ZH, Wei XS, Wei FW, Huang CM. 2009. Factors influencing interannual and intersite variability in the diet of *Trachypithecus francoisi*. *Int J Primatol.* 30(4):583–599.
- Zhou QH, Wei FW, Li M, Huang CM, Luo B. 2006. Diet and food choice of *Trachypithecus francoisi* in the Nonggang Nature Reserve, China. *Int J Primatol.* 27(5):1441–1460.
- Zhou X, Meng X, Liu Z, Chang J, Wang B, Li M, Wengel P, O-T, Tian S, Wen C, Wang Z, et al. 2016. Population genomics reveals low genetic diversity and adaptation to hypoxia in snub-nosed monkeys. *Mol Biol Evol.* 33(10):2670–2681.